Directed targeting of chromatin to the nuclear lamina is mediated by chromatin state and A-type lamins

Jennifer C. Harr,[1,2] Teresa Romeo Luperchio,[1,2] Xianrong Wong,[1,2] Erez Cohen,[1,2] Sarah J. Wheelan,[3] and Karen L. Reddy[1,2]

[1]Department of Biological Chemistry, [2]Center for Epigenetics, and [3]Department of Oncology Biostatistics and Bioinformatics, Johns Hopkins University, Baltimore, MD 21205

Nuclear organization has been implicated in regulating gene activity. Recently, large developmentally regulated regions of the genome dynamically associated with the nuclear lamina have been identified. However, little is known about how these lamina-associated domains (LADs) are directed to the nuclear lamina. We use our tagged chromosomal insertion site system to identify small sequences from borders of fibroblast-specific variable LADs that are sufficient to target these ectopic sites to the nuclear periphery. We identify YY1 (Ying-Yang1) binding sites as enriched in relocating sequences. Knockdown of YY1 or lamin A/C, but not lamin A, led to a loss of lamina association. In addition, targeted recruitment of YY1 proteins facilitated ectopic LAD formation dependent on histone H3 lysine 27 trimethylation and histone H3 lysine di- and trimethylation. Our results also reveal that endogenous loci appear to be dependent on lamin A/C, YY1, H3K27me3, and H3K9me2/3 for maintenance of lamina-proximal positioning.

Introduction

Recent evidence suggests that nuclear architecture influences gene regulation through establishment of large chromatin domains and through enrichment of regulatory and structural proteins within these regions (Misteli, 2005; Scaffidi and Misteli, 2006; Cremer et al., 2001, 2006; Fedorova and Zink, 2008; Elcock and Bridger, 2010; Ferrai et al., 2010; Van Bortle and Corces, 2012). One such domain, the nuclear periphery, is comprised of the inner nuclear membrane, resident inner nuclear membrane proteins, as well as underlying nuclear lamina and associated proteins. This region has been implicated in gene regulation, and various studies demonstrate that recruitment of genic regions (lamina-associated sequences [LASs]) to the nuclear periphery is sufficient to cause repression and silencing of associated genes (Finlan et al., 2008; Reddy et al., 2008; Zullo et al., 2012). More recently, molecular mapping of large chromatin regions in molecular contact with the nuclear periphery by DNA

adenine methyltransferase (Dam) identification (DamID) has identified large lamina-associated domains (LADs; 0.1–10 Mb) that dynamically associate with the nuclear lamina (Guelen et al., 2008; Peric-Hupkes et al., 2010). Moreover, cell state–specific association with the nuclear lamina appears to be involved in repression of many developmental genes, including the immunoglobulin heavy chain (*Igh*) locus (Kosak et al., 2002; Yang et al., 2005; Williams et al., 2006; Szczerbal et al., 2009; Meister et al., 2010; Peric-Hupkes et al., 2010; Yao et al., 2011; Lin et al., 2012). More recently, both LMNA/C (lamin A/C) and lamin B receptor have been implicated in tethering heterochromatin to the nuclear lamina during development (Solovei et al., 2013).

LADs have been reported to be repressive domains enriched in histone H3 lysine 9 di- or trimethylation (H3K9me2/3; Guelen et al., 2008; Wen et al., 2009; Towbin et al., 2012). In addition, two recent studies have implicated H3K9me2/3 in the positioning of chromatin at the nuclear lamina in murine cells and in *Caenorhabditis elegans* (Towbin et al., 2012; Bian et al., 2013). Intriguingly, the borders of LADs appear to be enriched

The Rockefeller University Press $30.00
J. Cell Biol. Vol. 208 No. 1   33–52
www.jcb.org/cgi/doi/10.1083/jcb.201405110

JCB   **33**

THE JOURNAL OF CELL BIOLOGY

in both H3K9me2/3 and H3K27me3 (histone H3 lysine 27 trimethylation) as well as CCCTC-binding factor (CTCF) binding sites; however, a role for the chromatin state found enriched in these regions in establishment and/or maintenance of LAD organization has not been thoroughly investigated (Guelen et al., 2008; Zullo et al., 2012; Meuleman et al., 2013; Van Bortle et al., 2013). It is of special note that these LAD borders, enriched in H3K27me3 and flanked by CTCF binding sites, are quite sharp and well delimited, suggesting an active mechanism to continually reestablish and maintain these regions.

Because many of the developmentally regulated variable LADs (vLADs) between cell types occur by shifting these LAD border regions, we hypothesized that the study of border regions of vLADS would enable a greater understanding of how the dynamic genome is reorganized at the nuclear periphery (Fig. 1; Peric-Hupkes et al., 2010). We therefore sought to elucidate factors and genic elements involved in positioning of chromatin to the nuclear periphery in mammalian cells, with a particular focus on dynamically reorganized border regions of LADs. This work identifies genomic regions containing developmentally regulated genes that reside in regions that are dynamically lamina associated depending on cellular state (vLADs) and, therefore, have regulated nuclear positioning. We have identified vLADs covering the *Ikaros* (*Ikzf1*) and *B cell CLL/lymphoma 11A* (*Bcl11a*) loci, which are positioned at the border of fibroblast (FB)-specific vLADs and are no longer associated with the lamina in pro–B cells. We have developed and used our tagged chromosomal insertion site (TCIS) system to examine single DNA sequences from these vLAD border regions for their ability to target and scaffold chromatin to the nuclear periphery. This approach has led to the discovery of a role for LMNA/C, YY1, H3K27me3, and H3K9me2/3 for targeting to the nuclear lamina of both ectopic and endogenous LADs.

Results

Developmental and cell type–specific genes are enriched in vLADS

The *Igh* locus, which itself comprises a vLAD, is lamina proximal and inactive in FB but is centrally disposed and active in pro–B cells where it is transcriptionally and recombinationally active (Fig. 1 A; Reddy et al., 2008). We hypothesized that there would be other vLADs between FB and pro–B cells that contain developmentally regulated genes. To determine whether such regions exist, we detected in vivo lamina–genome interactions by performing DamID in pro–B and FB cells (see Materials and methods; Vogel et al., 2007; Reddy et al., 2008). We determined LADs to be contiguous (>50 kb) regions exhibiting higher signal from Dam-LMNB1 (lamin B1) relative to the background control, Dam only ($\log_2$[Dam-LMNB1/Dam]), in mouse embryonic FBs (MEFs) and pro–B cells (Fig. 1, solid heavy blue or orange lines under histograms denote identified LADs; see Materials and methods; Venkatraman and Olshen, 2007; Zullo et al., 2012). These data are in agreement with previously published LAD data for MEFs (Fig. S1 A; Peric-Hupkes et al., 2010). In agreement with a previous study, we identified numerous vLADs between FB and pro–B cells that contain key developmental

and cell type–specific genes (Fig. 1; Peric-Hupkes et al., 2010). For this work, we focused on genes that were resident in LADs in FB but were not lamina-proximal in pro–B cells.

Not surprisingly, we demonstrate that the *Igh* locus is contained within one of these vLADs (Fig. 1 A; Reddy et al., 2008; Zullo et al., 2012). In addition, we have also determined that the key B cell development genes *Ikzf1* and *Bcl11a* are contained within FB-specific vLADs (but not in pro–B cells) as determined both by immuno-FISH and DamID protocols, consistent with their (active) roles in B cell development (Fig. 1, B and C; and Fig. S1 A). Therefore, these regions are ideal candidates for interrogating sequence-dependent mechanisms of positioning to the nuclear lamina. We also identified a region spanning the *Dnmt3a* gene, which is not in a LAD, but inactive (by array and quantitative PCR [qPCR] analyses), in our cell lines (Fig. 1 D). 3D immuno-FISH analyses confirmed that the disposition of these endogenous genomic regions in MEFs and pro–B cells are as expected (Fig. 1). It is important to note that the loci/regions we have identified in MEFs as lamina proximal by DamID are at the nuclear periphery in a majority of FB (65–80% have both alleles at the lamina), whereas these same regions display negative lamina association by DamID and an association rate of 30% in pro–B cells, reflecting the background level of "association" with the lamina by cytological measures. Both of these cell types are primary cells and may display different levels of association with the lamina when compared with data published from subcloned cancer-derived cell lines (Kind et al., 2013). Finally, gene expression microarray data from pro–B cells and FB demonstrate differential expression levels for *Bcl11a*, *Ikzf1*, and *Igh*, in agreement with previous studies and consistent with the nuclear lamina facilitating or reflecting a transcriptionally repressed state (unpublished data; Medina and Singh, 2005; Johnson et al., 2008, 2009; Reynaud et al., 2008; Heydarian et al., 2014).

Interestingly, we have noted that many vLADs are at LAD borders, suggesting that these regions may be especially important in dynamic genome reorganization (Peric-Hupkes et al., 2010 and unpublished data). The *Igh* locus is unusual in that the locus itself comprises the LAD (3 Mb) and the entire LAD reorganizes in pro–B cells, whereas *Ikzf1* and *Bcl11a* are more typical examples of vLADs, with only a portion of the LAD (proximal to the border) being lost in the permissive pro–B cell type (Fig. 1).

DNA sequences from vLAD borders target to the nuclear periphery

To elucidate the ability of specific LASs to direct targeting of sequences to the nuclear periphery, we integrated bacterial artificial chromosome (BAC) DNA constructs carrying sequences from FB-specific vLAD border regions covering the *Ikzf1* (RP23-349M24) and *Bcl11a* (RP23-30C14 and RP23-153C18) loci into the genome of NIH3T3-derived C57BL/6 FB (ATCC CRL-2752; Figs. S1 B and S2, A and B). As controls, a BAC from the distal, but internal, portion of the *Igh* locus (lamina-associated positive control, RP23-123N21) and another covering the *Dnmt3a* locus (non–lamina-associated negative control, RP23-364H6) were also used (Figs. 1 and S2; Zullo et al., 2012). These BACs were randomly cointegrated into FB cells with hygromycin-selectable *lacO* arrays, as previously described
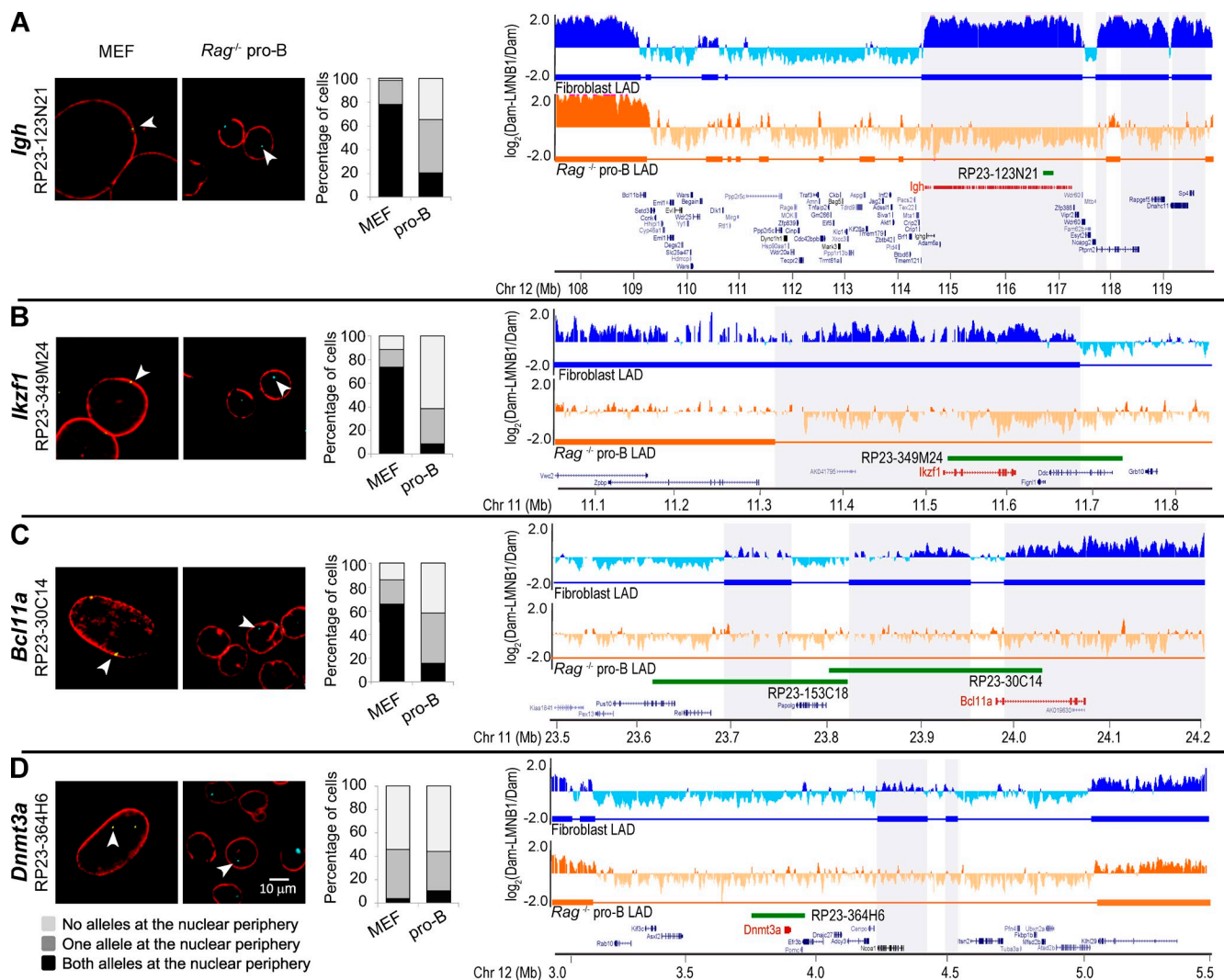
Figure 1. **Both FB and pro–B cell genomes contain vLADs.** (A–D) Shown are regions containing the *Igh*, *Ikzf1*, and *Bcl11a* loci from FB-specific vLADs. (left) Representative images of 3D DNA immuno-FISH of endogenous in FB and pro–B cells. FISH probes detecting the indicated regions are depicted (arrowheads), and the nuclear lamina is demarcated by LMNB1 (red). Quantitation of peripheral association was determined by overlap of FISH probe and LMNB1 ($n \geq 50$). (right) DamID detection of LADs $\log_2$(Dam-LMNB1/Dam) mean ratios from three experiments for FB (blue) and pro–B cells (orange). Traces above the 0 line indicate a region in a LAD. Solid blue and orange bars underscore LADs in FB and pro–B cells, respectively. Genes are indicated as transcripts (blue), and our gene of interest is red. BAC locations are indicated by green bars, and gray shading indicates an FB-specific vLAD. Chr, chromosome.

(Zullo et al., 2012). The *lacO* arrays serve as docking sites for EGFP-LacI, thus enabling quick identification by microscopy of the disposition of the integrations. An overlap of LMNB1 signal and an EGFP-LacI/*lacO* focus was scored as peripheral (Fig. S2, A and B). *lacO* arrays integrated alone served as a control for expected distribution of random integrations, and these were found at the periphery with a frequency of ∼30% (Fig. S2 B). Importantly, an integrated BAC covering the *Dnmt3a* locus is centrally disposed despite its inactive status, reminiscent of the disposition of the endogenous locus (Figs. S2 B and 1 D). We note that a previous study showed that the genomic region around the neuronal PAS domain 3 gene (*NPAS3*) was not in a LAD in FBs (though inactive) and was unable to reposition an ectopic site in this cell type, in agreement with our results for the genomic region around *Dnmt3a* (Zullo et al., 2012). Moreover, *NPAS3* is in a LAD in pro–B cells (unpublished data;

GEO accession no. GSE56990). These data suggest that, perhaps, sequences from domains that are not in an FB LAD are unable to confer lamina-proximal association in FB, regardless of transcription status or LAD status in alternate cell types. In contrast, BACs covering vLADs have a 60% (*Bcl11a*-1) to 80% (*Ikzf1*, *Bcl11a*-2, and *Igh*) propensity to be lamina proximal, mimicking the disposition of endogenous loci (Figs. 1 and S2 B). Given that these BAC LASs are able to mediate association of ectopic sites to the nuclear lamina, we next asked whether we could elucidate smaller sequences capable of such targeting. Both the *Ikzf1*- and *Bcl11a*-containing BACs demonstrating potential to direct to the nuclear periphery were further fragmented (*Ikzf1 (A–O)*; Figs. 2 A and S2 C), and these smaller potential *Ikzf1* LASs were randomly cointegrated with the aforementioned *lacO* arrays. The *Ikzf1* fragments tested ranged from 900 bp to 30 kbp and were derived from regions interior

to the vLAD border as well as those crossing and outside of the border regions (Fig. 2, A–C, *Ikzf1 (I)* and *(O)*). Interestingly, the fragments seem to show repositioning potential that correlated with the LAD status of the endogenous region (Fig. 2, B and C, gray bars). Noteworthy is the nonrelocating *Ikzf1 (F)* whose sequence falls in a break, or dip, in lamina association in an otherwise contiguous LAD region (Fig. 2, B and C, gray bars). Sequence from *Ikzf1 (O)* falls outside of a LAD, and it does not relocate to the periphery (Fig. 2, A–C, gray bars). We therefore hypothesize that *Ikzf1 (O)* lacks sequences sufficient to target (address) to the nuclear periphery, whereas the *Ikzf1 (I)* LAS retains this information. Similar results were obtained for the BAC containing sequences from the LAD border covering the *Bcl11a* locus (Fig. S2 D).

One caveat to this, and previously published experiments, is that the LASs tested have all been randomly integrated and likely represent many copies of the sequence at any given insertion site (Zullo et al., 2012; Bian et al., 2013). Therefore, it is difficult to determine whether an identified LAS was truly sufficient for targeting to the periphery or whether multiple copies of the LAS conferred a novel DNA or chromatin state that was itself a signal for compartmentalization. Intriguingly, many LADs contain duplicated genes or loci, for example, the *Igh* and *Cyp3a* loci, and are enriched in long interspersed nuclear elements, suggesting that multimeric sequences may be a signal for directing to the lamina (Zullo et al., 2012). However, there are regions of the genome that do not appear to be highly duplicated that are in a LAD (e.g., *Ikzf1* and *Bcl11a* LAD regions), and we therefore hypothesize that a single LAS may contain sufficient information to direct lamina-proximal targeting.

LAS from vLAD borders are sufficient to target to the periphery

To enable an experimental test of this hypothesis, we have developed a novel technique, TCIS, in which we can integrate a single DNA fragment of choice into the genome by directed recombination (Fig. S3 A). FB clone Y and 12 were identified as carrying a single integration site by qPCR and microscopy (immunofluorescence [IF] or live cell imaging of GFP-enriched foci). These parental clones display the "default" disposition of the single integrated TCIS system, which is away from the nuclear lamina (Fig. 2, B and C; and Fig. S3, B and C). We note that only a subset of the cells display EGFP-LacI foci detectable by 3D microscopy, as previously described (Belmont et al., 1999). Therefore, to ensure that we are able to measure disposition accurately using IF and EGFP-LacI foci as a readout, we demonstrated that 3D immuno-FISH to the *lacO* sequences reflected the same disposition as our IF strategy (Fig. S3 B). Although we do not know the integration sites, the TCIS region is not associated with the nuclear lamina by DamID analyses, thus the default association is away from the nuclear lamina (Fig. S3 C). Using this system, we are able to "switch" DNA segments into the TCIS system with high efficiency in as little as 5 d, with selection (Fig. S3 D). Thus, the TCIS system enables testing of a single noniterated LAS for its ability to target an ectopic genomic site to the nuclear periphery. Moreover, each LAS tested will be in the exact same genic location, thus mitigating

misinterpretation of results based upon possible position effects caused by differential integration sites.

The previously described *Ikzf1 (A–O)* fragments were therefore integrated into TCIS clone Y expressing EGFP-LacI to enable detection of disposition of the *lacO* sites (Fig. 2, A–C, black bars). These potential LASs in single copy showed relatively the same probability of targeting to the nuclear periphery in FB cells as they did in multiple copy random integrations (Fig. 2 C). The *Ikzf1 (I)* LAS (border) and a control from *Igh* LASs were tested in both of our clones Y and 12 (Fig. 2, D and E; Zullo et al., 2012); additionally, fragments from broader border regions near *Bcl11a* were integrated into clones 12 and Y, and similar results were obtained (Fig. S2 E). The transitional *Ikzf1 (I)* LAS, which covers the outermost edge of the *Ikzf1* LAD border region, was then further dissected to identify specific DNA elements with roles in establishing and/or defining a LAD. Specifically, 2.5-kbp subfragments covering the entire *Ikzf1 (I)* were switched into clone Y. The smaller *Ikzf1 (I)* LAS fragments comprised of sequences derived from regions adjacent to borders, but outside of LADs, are unable to mediate repositioning (Fig. S4 B). We note that *Ikzf1 (I)* LAS fragments 3 and 4 straddle the defined border region. These results indicate that there is both a sharp edge delimiting lamin-associated regions and that sufficient information required for repositioning to the nuclear periphery resides at or inside LAD boundaries in small LASs (<2.5 kbp).

Cell type–specific transcription factors and proteins involved in nuclear architecture and scaffolding are involved in sequence targeting

We next aimed to determine enrichment of protein binding motifs within *Ikzf1 (A–E and G–I)* LAS that would serve to identify potential protein candidates for further functional analyses. An initial search using MEME and TomTom identified YY1 (Ying-Yang 1), CTCF, and cKrox/ThPOk/Zbtb7b (as well as other BTB/POZ domain proteins) binding site motifs as among those enriched in these sequences (see Materials and methods; Fig. S4, C and D). Not surprisingly, we also identified several binding sites for specific B cell development proteins (not depicted). Both CTCF and Zbtb7b binding site motifs were previously identified in LADs/LAS (Guelen et al., 2008; Zullo et al., 2012). Intriguingly, YY1 is known to have roles in genome regulation in many cell types, including both gene activation and repression, and has been implicated to recruit polycomb repressive complex 2 (PRC2) to chromatin to enable H3K27me3 (Satijn et al., 2001; Atchison et al., 2003; Caretti et al., 2004; Srinivasan and Atchison, 2004; Liu et al., 2007; O'Meara and Simon, 2012; Pan et al., 2013; Atchison, 2014).

We next undertook to identify all potential YY1 binding sites in LAD border regions via pair-weighted matrix motif analyses. Specifically, we analyzed the disposition of predicted YY1 and CTCF binding sites (Fig. S4, C and D) over chromosomes 11 and 12 using MEME Suite and Genometricorr (Claeys et al., 2012; Favorov et al., 2012). Using the MEME-identified motifs, we generated maps of sites along each fragment using the MAST algorithm (Fig. S4 C). In addition, because the output of MEME
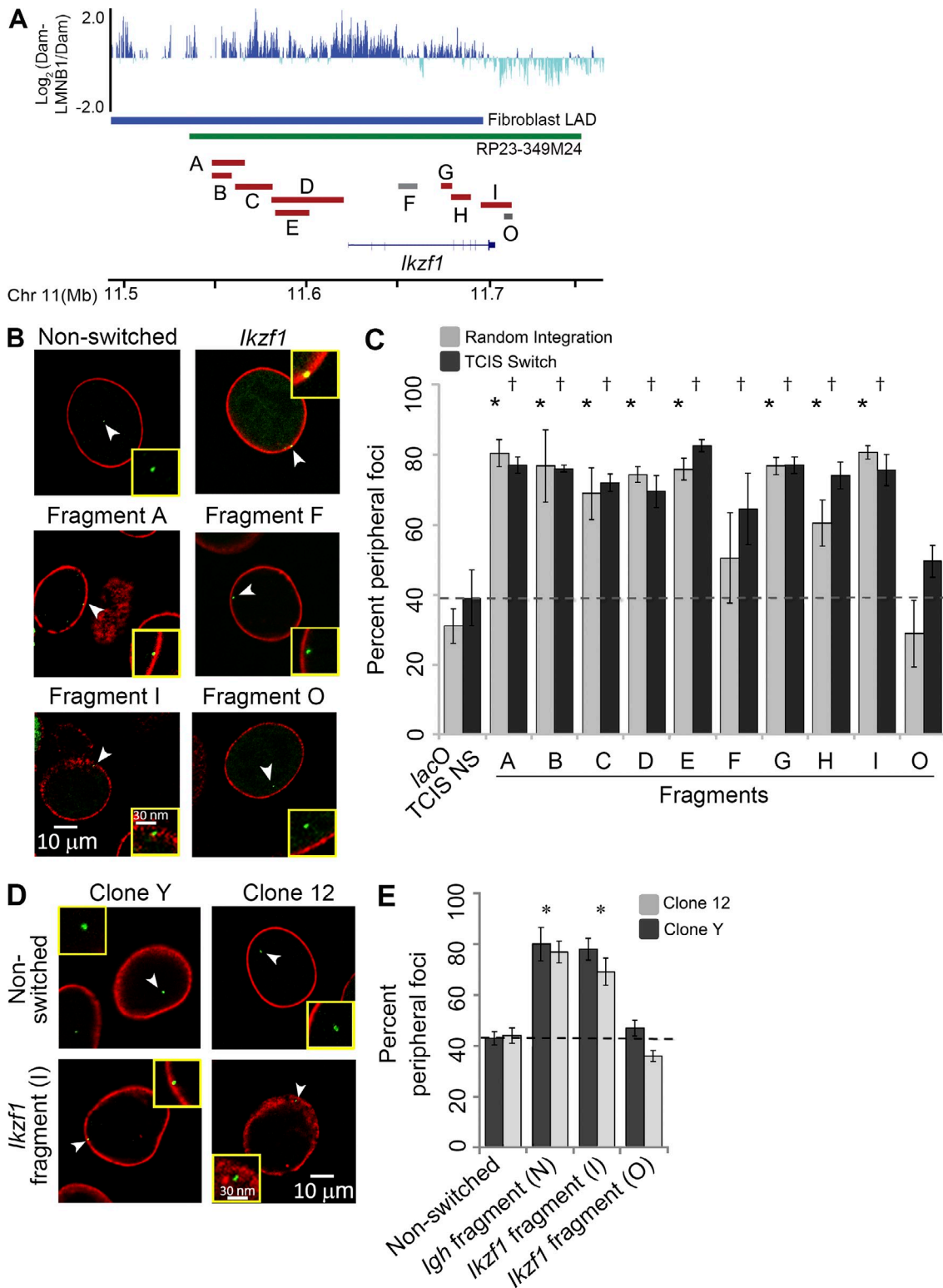
Figure 2. **Ikzf1 LASs target to the nuclear periphery in FB.** (A) *Ikzf1 (A–I* and *O)* fragments span the border region of the FB-specific *Ikzf1* vLAD. Histograms are $\log_2(\text{Dam-LMNB1/Dam})$, and the blue bar underscores the LAD. The *Ikzf1* locus (blue) and overlapping BAC used to generate the smaller fragments are shown (green). *Ikzf1* LASs are red, and nonassociating fragments are gray. (B) Representative images showing the disposition of *lacO* arrays (arrowheads, green) and LMNB1 (red) in the original TCIS clone as well as nuclei harboring randomly integrated *Ikzf1* BAC fragments (top) or TCIS clones with site-specific recombination of *Ikzf1 (A, F, I,* and *O).* The inset shows 300× magnification. (C) Quantitation of peripheral association was determined by overlap of EGFP-LacI foci and LMNB1 ($n \geq 50$). Fragments were tested for their ability to target to the nuclear periphery by random integration or by directed integration (TCIS). Error bars indicate SD. $P \leq 0.001$ (asterisks show random integration, and crosses are TCIS switch). NS, nonswitched. (D) Representative images of IF for the disposition of *Ikzf1 (I)* or *Igh (N)* LAS recombined into the TCIS sites in clones Y and 12. Arrowheads show EGFP-LacI binding *lacO* arrays (green) at the TCIS site and LMNB1 (red). Insets are 300× magnifications. (E) Quantitation of peripheral association of *Ikzf1 (I)* or *Igh (N)* LAS in clones Y and 12 ($n \geq 50$, $P \leq 0.05$). Dotted lines are approximate peripheral association of the nonrecombined TCIS insert.
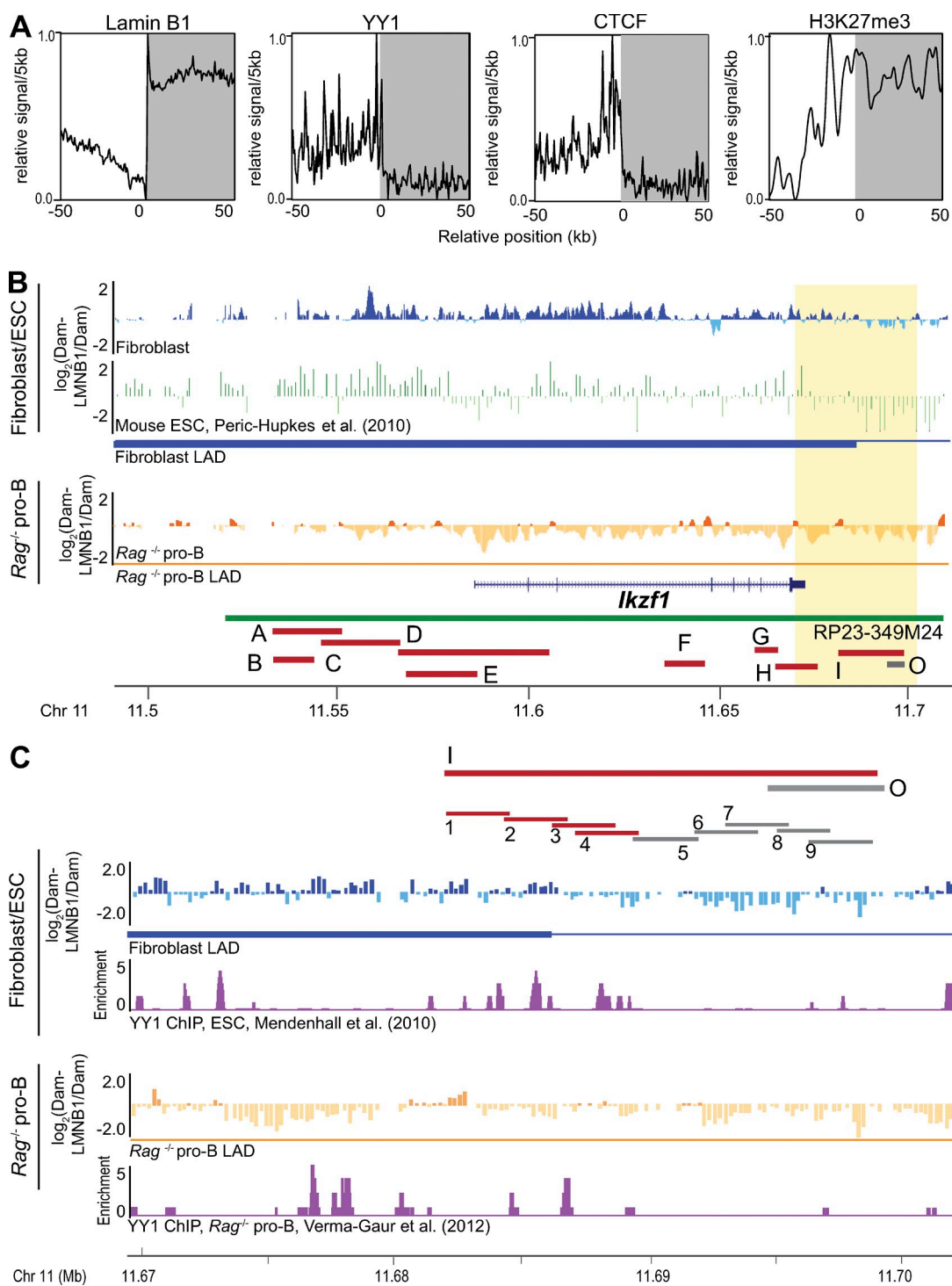
Figure 3.   **YY1 binding sites are enriched in LAS.** (A) Profiles of aligned LAD border regions (chromosomes [Chr] 9–14; left and mirrored right border regions combined) are shown for LMNB1 binding, YY1, and CTCF binding site density and H3K27me3. To align LAD borders, genome-wide positions of all analyzed features were converted to coordinates relative to the nearest border. Gray area and positive coordinates, inside LADs; white area and negative coordinates, outside LADs. (B) DamID histograms in FB (blue), ESC cells (green; GEO accession no. GSE17051; Peric-Hupkes et al., 2010), and pro–B cells (orange). Histograms are log$_2$(Dam-LMNB1/Dam), and a positive signal indicates a LAD region. The solid blue and orange bars underscore LADs. The *Ikzf1* locus (blue) and BAC used to generate the smaller fragments (green) are shown below the fragments. LASs are depicted in red, and nonrepositioning fragments are depicted in gray. (C) Depicts magnification of the *Ikzf1* LAD border (light yellow from B). Subfragments (1–9) of the *Ikzf1* (I) LAS are shown relative to ChIP-Seq data from ESC, and pro–B cells show YY1 binding site enrichment (YY1, GEO no. GSM628031; pro–B, GEO no. GSM1002560; Mendenhall et al., 2010; Verma-Gaur et al., 2012).

simply indicates a statistically significant enrichment of a given motif, we next analyzed the fold enrichment of identified motifs in our fragments relative to random regions of chromosome 11 away from LAD borders from either MEME-generated motifs or from the transcription factor binding motif databases Factorbook and JASPAR (Fig. S4 D; Sandelin et al., 2004; Wang et al., 2012; Mathelier et al., 2014). For comparison, we show enrichment of these MEME and Factorbook motifs on known YY1 responsive elements surrounding the *Surf1/2* gene (*Surfeit locus protein 1 and 2*) and the Emu enhancer from the *IgH* locus size matched to fragment I, for comparison (Fig. S4 D; Cole and Gaston, 1997). Using MotifSuite, we estimate an approximately twofold enrichment of YY1 binding sites at LAD borders (±10 kb) relative to chromosomal background (unpublished data; Claeys et al., 2012). Finally, the statistical correlation package Genometricorr indicates that YY1 binding sites, either derived from our MEME analyses or from the Factorbook database of binding motifs, are more enriched relative to LAD borders compared with what would be expected by random chance (P < 0.001; Favorov et al., 2012).

These initial lead candidate analyses led us to next identify actual YY1 occupancy relative to LADs. Leveraging publicly available data of YY1 binding and LMNB1-DamID (e.g., LAD) maps in embryonic stem cells (ESCs) along with our data and publicly available data in pro–B cells, we found that high peaks of YY1 binding often correlated with LAD boundaries (Fig. 3 A; Mendenhall et al., 2010; Peric-Hupkes et al., 2010; Vella et al., 2012). We note that in the *Ikzf1*, *Bcl11a*, and *Igh* loci, the LAD configuration in ESCs mimics those seen in FB (Fig. 3 B, top). In addition, we note that the smaller relocating fragments (fragments 1–4), some of which, by bioinformatics analyses, were not identified as enriched in YY1 binding sites, nonetheless display YY1 occupancy in both non–B cell types, in this case ESCs, and pro–B cells (Fig. 3 C). It is thus very important to note the obvious: there are a large number of regions actually occupied by YY1 both inside and, more predominantly, outside of LAD border regions and, in the case of previously published results in ESC cells, YY1 occupancy is often associated with active promoter regions (Fig. 3 A; Vella et al., 2012). Interestingly, although *Ikzf1* is in a LAD in ESCs, it is not in pro–B cells, yet in both cell types, these regions have demonstrated YY1 binding (Fig. 3 C). This likely reflects both the diversity of YY1 functions and its potential dual roles in regulating these regions. We also note, as has been previously reported, that we find CTCF binding motifs to be enriched at LAD borders (Figs. 3 A and S4, C and D; Guelen et al., 2008). In all cases, the putative and determined binding sites were shown to be enriched in LAD border regions; however, it is quite evident that these regions are far from the only regions bound by these factors. Given these and previous data, we suspected that targeting to the lamina may depend upon on a combination of cell type–specific factors (such as BTB-POZ domain proteins; Fig. S4, C and D) as well as epigenome/genome organizers, such as YY1, PRC2 components (e.g., EZH2), lamins, and/or CTCF (Fig. S4 E). However, it was also clear from these analyses that simply trying to determine bioinformatically (motif or occupancy analyses) the roles of these proteins in LAD establishment would be problematic.

To more rigorously determine the role of the identified candidate proteins in LAD establishment and/or maintenance, we used a targeted shRNA-mediated knockdown strategy (Fig. 4). Specifically, a test fragment from the *Ikzf1* vLAD border (LAS I) and a control fragment from the *Igh* vLAD (LAS N) were introduced into TCIS insertion sites in clone 12 and Y, and these same cells were then subjected to shRNA-mediated knockdown of either proteins previously identified to be important for de novo lamina association (Zbtb7b, HDAC3, and Lap2-β) as well potential novel players based on the literature (LMNA/C) or in this study (CTCF, YY1, and the PRC2 component EZH2). We determined the disposition of the LAS before shRNA-mediated knockdown with either an off-target shRNA control or with the indicated protein target (Fig. 4). Lap2-β and HDAC3 shRNA-mediated knockdowns led to substantial cellular death and were, therefore, not able to be analyzed with confidence; however, the remainder of the constructs appeared to have little effect on cell viability within the time frame used by our assays (Fig. S5 A). Interestingly, all of these knockdowns, with the prominent exception of LMNA, led to the loss of peripheral association of targeting fragments (Fig. 4, B and C, P < 0.05). It is important to note that the LMNA knockdown construct specifically knocks down LMNA, whereas the LMNA/C construct knocks down both LMNA and LMNC (Fig. 4 A). Given these results, it is tempting to speculate that LMNC, but not LMNA, is important for maintaining lamina-proximal positioning.

We next asked whether the proteins demonstrated to impact LAS-directed targeting to the nuclear lamina also affected endogenous LAD organization. Both LMNA/C and YY1 perturbation reduced the association of endogenous LADs containing *Ikzf1*, *Igh*, and *Bcl11a* with the nuclear lamina as determined by 3D immuno-FISH (Fig. 4 D, P < 0.005). In contrast, disruption of Zbtb7b only affected the association of the *Igh* locus with the lamina with any degree of statistical significance (Fig. 4 D). Collectively, these data suggest that peripheral targeting and maintenance of lamina association of these regions is dependent on both LMNA/C and YY1. Again, ablation of LMNA alone had no effect on the disposition of endogenous loci.

Because YY1 shRNA-mediated knockdown affected the nuclear disposition of both ectopically recruited TCIS sites and endogenous loci (Fig. 4), we specifically tested whether YY1 is sufficient to target an ectopic site to the nuclear periphery. To enable such an experimental test, we expressed a YY1-EGFP-LacI fusion protein in our clones Y and 12 (harboring the original nonrelocating vector sequence) in the presence or absence of IPTG, thus allowing for regulated accumulation of YY1 at the integration site (Fig. 5, C and D). The YY1-EGFP-LacI fusion protein displayed the same punctate distribution in the nucleus as endogenous YY1, making identification of the bound *lacO* array difficult in most cells (Fig. S5 B). We note, however, that some cells express the fusion at lower levels and were thus able to be assayed by IF; in these cells, the YY1-EGFP-LacI loci colocate with YY1-enriched foci (Fig. S5 C). To enable clear identification of the disposition of these YY1-bound TCIS insertions, we performed 3D immuno-FISH and measured their association with the nuclear periphery using LMNB1 to demarcate the nuclear periphery (Fig. 5, C and D). Although these integrations

Figure 4. **Knockdown of Zbtb7b, CTCF, YY1, EZH2, or LMNA/C leads to a loss of peripheral association of LAS.** (A) Immunoblot analysis of protein lysates from TCIS lines Y and 12, harboring LAS *Ikzf1 (I)* (Ik) or *Igh (N)* and control nonswitched (NS) with either off-target or target shRNA as indicated to the left of each blot. (B and C) Quantitation of IF testing the disposition of *lacO* and LMNB1 in TCIS clones harboring the *Ikzf1 (I)* (B) or *Igh (N)* (C) LAS, after 4-d treatment with the indicated shRNA (*n* ≥ 50; *, P ≤ 0.001). (D) Quantitation of 3D DNA immuno-FISH for BAC probes to the indicated endogenous LAD regions in MEFs treated with the indicated shRNA constructs (*n* ≥ 50; *, P ≤ 0.05). Error bars indicate SD. Dotted lines are approximate peripheral association of the nonrecombined TCIS insert.
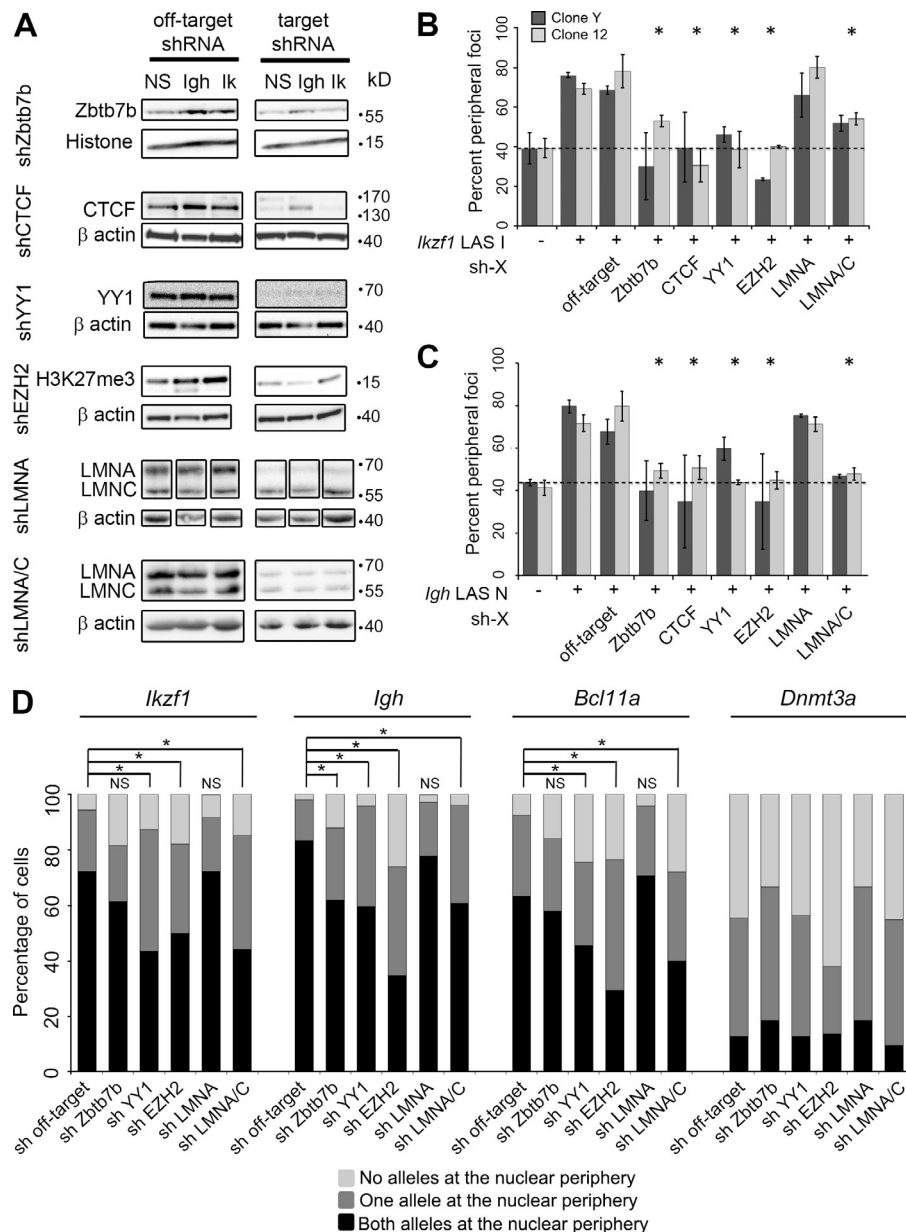
are centrally disposed when bound by EGFP-LacI, nearly 80% of the YY1-EGFP-LacI foci are at the nuclear periphery after 24 h. This finding is also borne out by DamID analyses of YY1-bound TCIS loci (Fig. 5 E, *Ikzf1 (I)* or −IPTG, black bars) compared with controls (Fig. 5 E, nonswitched and +IPTG, black bars). We note that LAS I switched into TCIS also displays lamina association by DamID (Fig. 5 E). In these experiments, relative lamina association and efficacy of the DamID protocol was monitored in the same experiment by PCR using *Igh* primers internal to the *Igh* vLAD. Specificity of the protocol was measured by using primers to detect a region in a small "dip" between and proximal to LAD regions (Fig. 5 E; Wen et al., 2012). Importantly, simply overexpressing YY1 does not lead to repositioning of ectopic TCIS integrations (without recruitment to the *LacO* array, ±IPTG) or the control (dip) region to the lamina, indicating that simply overexpressing YY1 does not cause global reorganization to the nuclear lamina or even spreading

into LAD proximal regions (dip; Fig. 5). An accumulation of the YY1 protein, at a discrete site, is therefore sufficient to target to the nuclear periphery. In contrast, tethering of Zbtb7b is not sufficient to drive these regions to the nuclear periphery, even though the fusion protein is expressed, recruited to TCIS, and appears to be functional, as assayed by reduction in *col1a1* (*collagen, type I, α 1*) and *fibronectin* gene expression (Fig. 5, A–D; Widom et al., 1997; Renard et al., 2008). Interestingly, YY1 is not normally enriched at the nuclear lamina, although we do detect faint rim staining upon longer exposure when detecting endogenous YY1 by IF (Fig. S5 D). However, we note that although YY1 is not obviously enriched at the nuclear lamina in most cells, H3K27me3 and Hoechst-stained heterochromatin is indeed enriched in the region underlying the lamina, enhanced in those cells overexpressing YY1 (Fig. S5, B and C).

Interestingly, there are previous studies indicating that recruitment of YY1 leads to association with pericentromeric
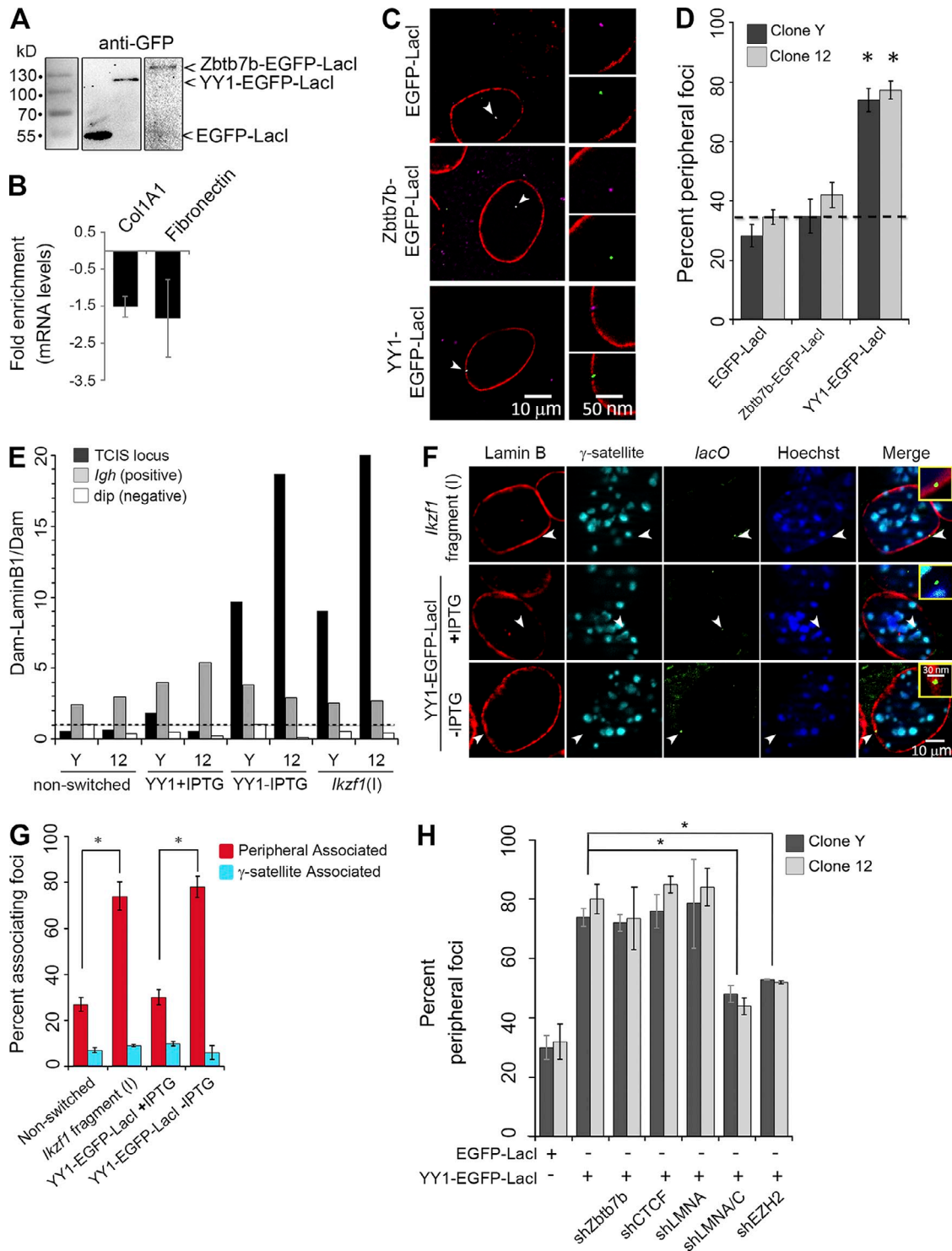
Figure 5. YY1 targets chromatin to the nuclear periphery. (A) Expression of YY1 and Zbtb7b fusions to EGFP-LacI were verified by immunoblotting by detection with α-GFP. (B) qRT-PCR of Col1A1 and fibronectin in FB cells overexpressing Zbtb7b-EGFP-LacI. (C) Representative images of 3D DNA immuno-FISH. EGFP-LacI, YY1-EGFP-LacI, or Zbtb7b-EGFP-LacI fusion proteins detected by α-LacI (magenta, arrowheads) colocalize with the TCIS insert site (*lacO* probe, green, arrowheads) and LMNB1 (red). (D) Quantitation of 3D DNA immuno-FISH for *lacO*/LacI position in two TCIS clones (*n* ≥ 50; *, P ≤ 0.001). Dotted line is the approximate peripheral association of the nonrecombined TCIS insert. (E) qPCR analysis of Dam-LMNB1/Dam in clone Y and 12 under the indicated conditions. A value >1 for (Dam-LMNB1/Dam only) indicates enrichment. Primers to the TCIS locus, the *Igh* locus (positive control), and a non–lamina-associated region, dip (negative control), were used for amplification. The data shown are from a single representative experiment. Dotted line is a ratio of 1 for Dam-LaminB/Dam. (F) Representative images of 3D DNA immuno-FISH in clone Y containing either *Ikzf1 (I)* LAS or YY1-EGFP-LacI (±IPTG). LMNB1 (red), γ-satellite (cyan), *lacO* probe (green), and Hoechst (blue) are shown. Arrowheads show the disposition of *lacO* arrays. Insets are 300× magnifications. (G) Quantitation of 3D DNA immuno-FISH for *lacO* position in relationship to both the nuclear lamina and γ-satellite DNA with either *Ikzf1 (I)* LAS integrated or YY1 bound (*n* ≥ 50; *, P ≤ 0.001). (H) Quantitation of the disposition of *lacO* sites by 3D immuno-FISH analysis in clone 12 and Y overexpressing YY1-EGFP-LacI (−IPTG) before and after shRNA-mediated knockdown (as indicated; *n* ≥ 50; *, P ≤ 0.001). Error bars indicate SD.

Figure 6. **H3K27me3 enriched at endogenous LAD borders and YY1-bound TCIS.** (A and B) H3K27me3 enrichment at LAD borders (GSE48649; Simon et al., 2013). The entire FB LAD is shown for *Ikzf1* and *Igh* to enable visualization of both borders, and the blue bar underscores a LAD region determined by LAD histograms (log$_2$(Dam-LMNB1/Dam)). The genes are shown (blue), and the *Ikzf1* vLAD border region tested in this study is highlighted in yellow. Primers used for ChIP to the *Igh* locus are indicated (orange). (C) Magnification of the 20-kb edge of the FB-specific vLAD containing *Ikzf1*. LAS (magenta) and nontargeting fragments (gray) are shown above H3K27me3 histograms. (D) ChIP analysis of YY1 recruited to the TCIS locus (±IPTG). Enrichment of H3K9me2, H3K9me3, and H3K27me3 at the indicated locus is shown as a percentage of input. Error bars indicate SD. Chr, chromosome.
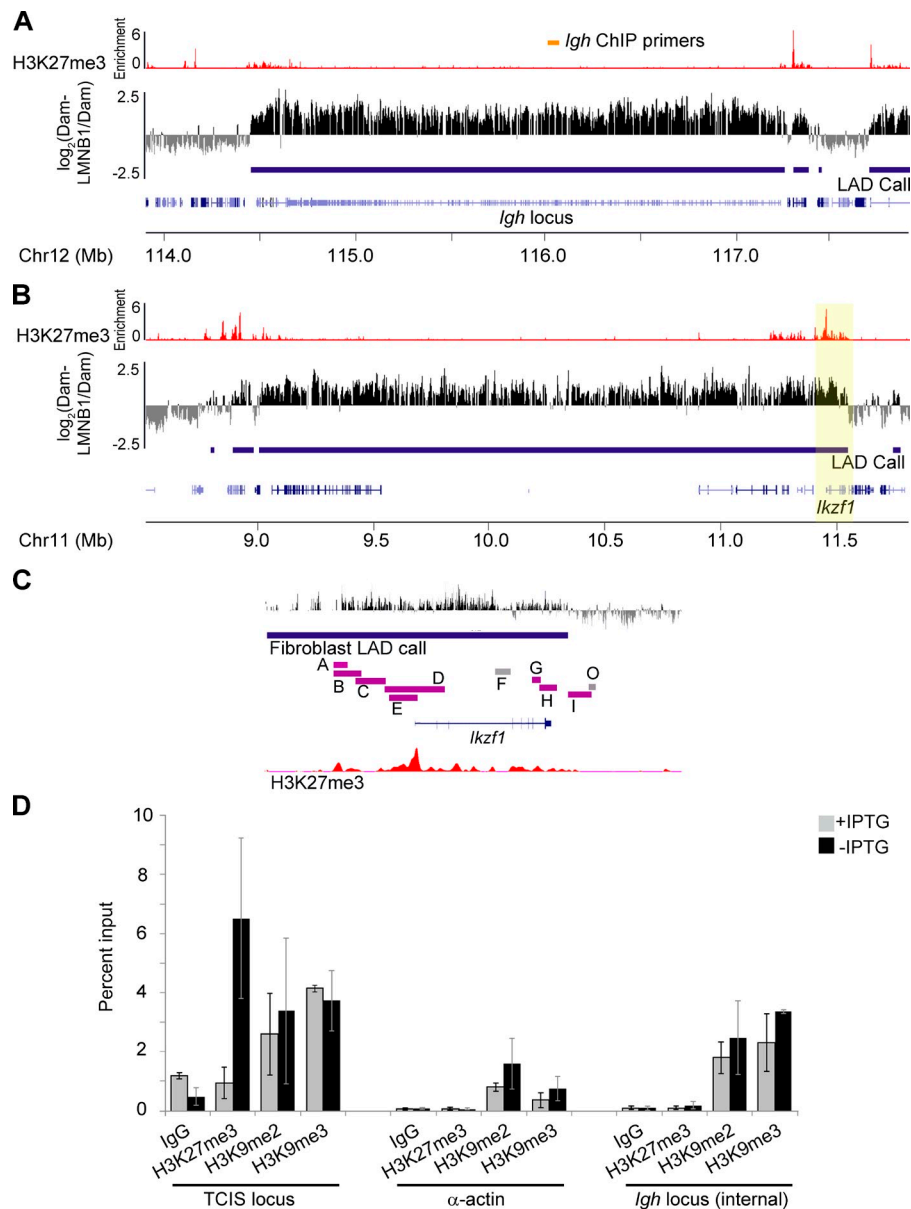
heterochromatin (Shestakova et al., 2004; Josse et al., 2012). We therefore asked whether directed recruitment of YY1 led to the association of the TCIS site with these domains by using either 3D immuno-FISH or IF assays to determine the amount of colocalization of the YY1-bound TCIS locus with either pericentromeric γ-satellite DNA or with the centromeric protein CENP-A (Fig. 5, F and G; and Fig. S5, E and F). We observe no increase in association with either of these subnuclear regions. Collectively, these data indicate that YY1 is able to direct recruitment of an ectopic site to the nuclear lamina and that this recruitment is independent of association with pericentromeric or centromeric heterochromatin domains.

Given that YY1 recruitment to TCIS is sufficient to target that region of the genome to the nuclear lamina, we next asked whether such repositioning was dependent on putative YY1 interactors and/or lamina proteins. Both CTCF and BTB-POZ proteins have been implicated to interact with YY1 (Donohoe et al., 2007; Zlatanova and Caiafa, 2009; Boulay et al., 2012).

shRNA-mediated knockdown of LMNA/C was able to prevent or disrupt YY1-mediated tethering to the nuclear lamina, although LMNA knockdown alone was not sufficient to cause disruption of this interaction (Fig. 5 H). In contrast, knockdown of either Zbtb7b or CTCF did not disrupt peripheral association, indicating either that these proteins are not involved in this process or that YY1 recruitment is able to bypass their functional requirements (Fig. 5 H). Nonetheless, these data show that YY1-mediated recruitment to the nuclear lamina depends on LMNC and, possibly, LMNA/C levels.

Intriguingly, H3K27me3 has been reported to be enriched at LAD borders but not LAD interiors (Guelen et al., 2008). Using publicly available data identifying H3K27me3 in MEFs (GEO accession no. GSE48649), we also note that there is a striking enrichment of H3K27me3 at the border of the LADs containing the *Ikzf1*, *Igh*, and *Bcl11*a loci and more generally at LAD borders (Fig. 6, A and B; and Fig. 3 A; Simon et al., 2013). These H3K27me3 modifications overlap with our relocating

fragments (Fig. 6 C). We next asked whether YY1 recruitment to the TCIS locus mirrored what is observed at endogenous LAD borders, namely the accumulation of H3K27me3-modified chromatin at the insert site (Fig. 6, B and C). By chromatin immunoprecipitation (ChIP), we detected strong enrichment of H3K27me3 upon recruitment of YY1 and found, additionally, that our inserts harbor H3K9me2/3 modifications independent of YY1 recruitment (Fig. 6 D). We note that the antibodies used for detecting the H3K9 methyl modifications have significant cross-reactivity between dimethyl and trimethyl variants, and so, we describe our data in terms of H3K9me2/3 (Peach et al., 2012). Intriguingly, a recent study indicated that H3K9 methyl status may determine chromosomal positioning at the lamina of ectopic insertion sites (Bian et al., 2013). In addition, genome-wide analyses in *C. elegans* have shown a correlation between H3K9me1/2/3 enrichment and LAD regions (Towbin et al., 2012). Moreover, H3K9me2 has been previously reported to play a role in LAD organization and in regulation of the *Igh* locus, and we also detected enrichment of this modification in the interior of the LAD comprising the *Igh* locus (Fig. 6 D; Johnson et al., 2004). As expected, these more interior primers of the *Igh* LAD did not detect an enrichment of H3K27me3, indicating that this modification is present at border regions of LADs, but not the interior, in agreement with our and others' analyses of H3K27me3 ChIP-seq signatures relative to LAD borders (Figs. 3 A and 6 D; Guelen et al., 2008). We therefore conclude that our YY1-bound TCIS system likely recapitulates the endogenous chromatin state of LAD borders in that they have both H3K9me2/3 and H3K27me3 modifications.

YY1 has been shown to act as both a negative and positive transcriptional regulator (Thomas and Seto, 1999); however, one reported role is in recruiting PRC2 to mediate transcriptional repression (Basu and Atchison, 2010; O'Meara and Simon, 2012; Basu et al., 2014). Previously, we showed that reduction in the PRC2 histone methyltransferase component EZH2, which trimethylates histone H3 on lysine 27, led to the loss of peripheral association of a LAS fragment (Fig. 4). In addition, disruption of EZH2 prevented YY1-mediated recruitment to the nuclear lamina, indicating that H3K27me3 is necessary for this repositioning as well (Fig. 5 H). We note, however, that overexpression of YY1 concomitant with disruption of EZH2 in the same cells led to a substantial decrease in cell viability (unpublished data). As a separate test to determine whether H3K27me3 was required for the YY1-mediated repositioning, we treated TCIS clones with either relocating LAS fragments recombined into the locus (Fig. 4) or bound by YY1 (Fig. 5) with 3-deazaneplanocin (DZNep). DZNep is an indirect inhibitor of S-adenosyl-methionine–dependent methylation that disrupts EZH2 function, thus blocking H3K27me3 deposition. In addition, there are reports that, depending on the study, implicate DZNep in the reduction of H3K4me3, H4K20me3, and at higher concentrations, H3K9me3 (Fig. 7 A; Fiskus et al., 2009; Miranda et al., 2009; Lee and Kim, 2013). We used DZNep in addition to shRNA-mediated knockdown of the EZH2 methyltransferase because loss of EZH2 might lead to destabilization of some of the YY1 containing complexes, thus making results from such an experiment difficult to interpret. We note that treatment with

5 µM DZNep resulted in modest effects on cell proliferation at 24 h of treatment (the time point used for our assays), but the cells appeared to be otherwise healthy (Fig. S5 G). Strikingly, lamina association driven by LASs are disrupted when treated with DZNep (Fig. 7, B and C) as they are with EZH2 knockdown (Fig. 4, B and C), indicating that their repositioning is dependent on H3K27me3. Intriguingly, DZNep treatment affected all LAS fragments similarly, including the *Igh(N)* LAS, indicating that either H3K27me3 is involved in initiating lamina association regardless of LAS origin or that our treatments also affected other histone modifications necessary for repositioning, especially H3K9me2/3 (see following paragraph; Fig. 7 C; Towbin et al., 2012; Bian et al., 2013). However, in support of a strong role for H3K27me3 in LAS-directed repositioning, shRNA-mediated knockdown gave similar results for these same LAS fragments (Fig. 4 C). Similarly, DZNep treatment of either YY1-bound loci or endogenous LADs resulted in their movement away from the nuclear lamina, again similar to our findings with shRNA-mediated knockdown of EZH2 (Fig. 7, D and E). Collectively, these results suggest that H3K27me3 is necessary to target to and maintain proximity to the nuclear lamina.

As previously mentioned, there are studies in the literature implicating histone H3K9me2/3 modifications in recruitment of domains to the nuclear lamina. We also note that our TCIS system harbors H3K9me2/3-modified chromatin, as has been previously reported for these types of arrays (Janicki et al., 2004; Towbin et al., 2012; Bian et al., 2013). Taking these findings into consideration, we next asked whether the association with the nuclear lamina might be dependent on both types of modifications—a potential bivalent heterochromatin signal. Intriguingly, H3K9me2/3 modifications appear to be broadly distributed across LAD domains (unpublished data; Towbin et al., 2012), although H3K27me3 modifications appear to be restricted (relative to LADs) at the border regions (Fig. 6; Guelen et al., 2008). These border regions may represent regions where the genome is constantly reestablishing LAD boundaries as indicated by the preponderance of active promoters immediately flanking LADs (Guelen et al., 2008). To test whether repositioning of ectopic regions to the nuclear lamina requires H3K9me2/3 modifications, we used the inhibitor BIX-01924 to block histone dimethylation at lysine 9 of H3 (Kubicek et al., 2007; Bian et al., 2013). We chose to use this inhibitor because, despite our best efforts, we were unable to find an shRNA construct for G9a (the methyltransferase responsible for H3K9me2; Lachner and Jenuwein, 2002) that worked without significant cell death (unpublished data). Western blots show that treatment with 5 µM BIX-01924 leads specifically to inhibition of H3K9me2 but not H3K9me3 (Fig. 8, A and B). Initially, we subjected cells harboring our TCIS system with the *Ikzf1 (I)* LAS or with YY1 bound to treatment with the inhibitor for 24 h, and, although we saw significant down-regulation of H3K9me2, we were unable to reliably detect loss of lamina association (Fig. 8, C and D). Interestingly, another study also tried using BIX-01924 to disrupt lamina associations through down-regulation of H3K9me2 but also were unable to detect loss of association; however, the authors noted that their assays to detect lamina association were designed to detect within 0.5 µm of the nuclear lamina, and therefore, they

Figure 7. **DZNep treatment leads to loss of peripheral targeting.** (A) Immunoblot analysis of H3K27me3 in clones 12 and Y ±5 μM DZNep treatment for 24 h. (B) Representative images of clone Y harboring the *Ikzf1 (4)* LAS, ±DZNep treatment. EGFP-LacI foci (green, arrowheads) are shown relative to LMNB1 (red) and H3K27me3 (magenta). Insets are 300× magnifications. (C) Quantitation of IF for DZNep treatment of clone Y harboring *Igh (N)* and *Ikzf1 (4)* LAS and a nontargeting fragment *Ikzf1 (8)* ($n \geq 50$; *, $P \leq 0.05$). (D) Quantitation of IF of 24-h, 5 μM DZNep-treated clones Y and 12 expressing EGFP-LacI or YY1-EGFP-LacI ($n \geq 50$; *, $P \leq 0.001$). Error bars are SD. (E) Quantitation of 3D DNA immuno-FISH for the indicated endogenous loci in MEFs treated with 5 μM DZNep (24 h) MEFs ($n \geq 50$; *, $P \leq 0.05$).
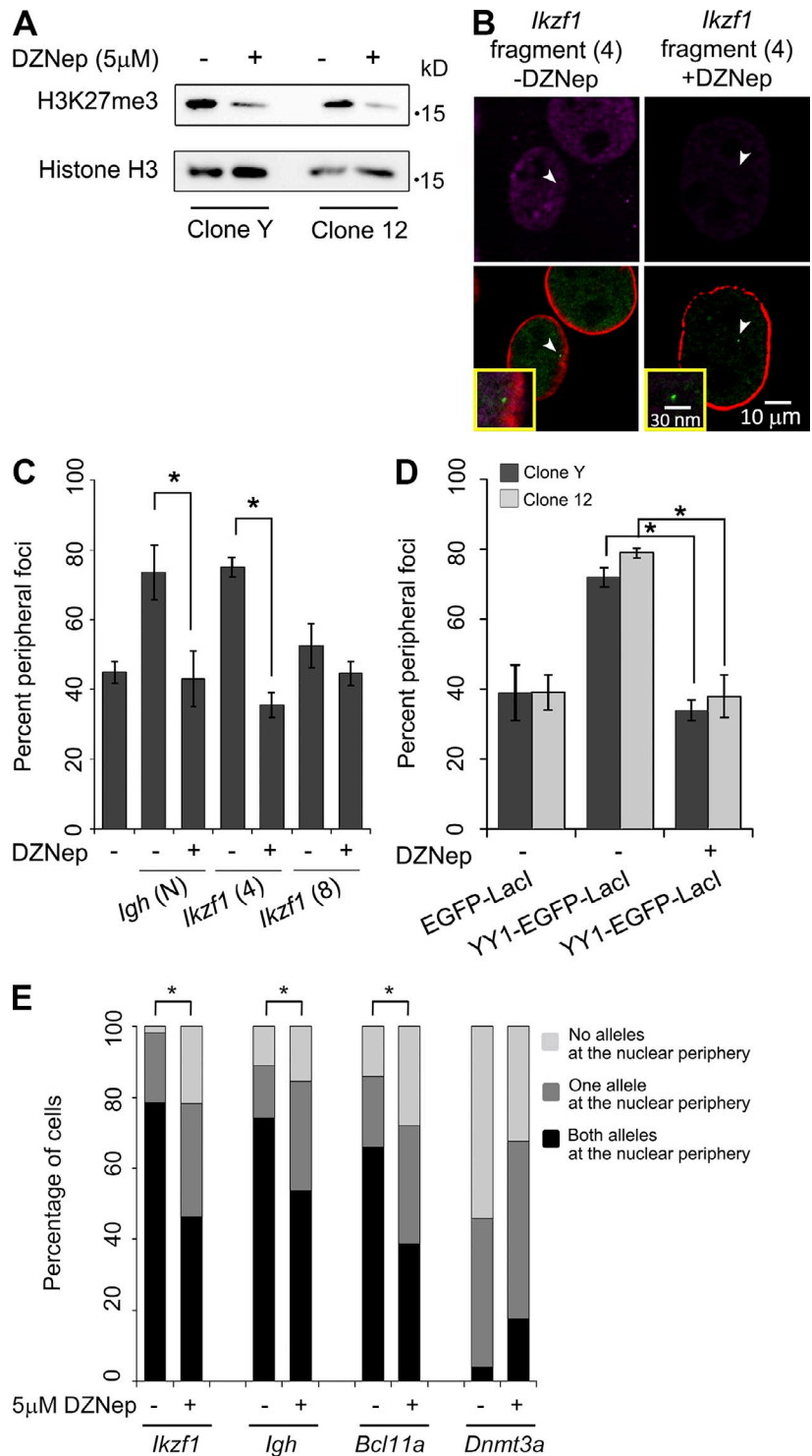
may have missed a more subtle loss of association (Bian et al., 2013). Another study clearly implicated this modification with recruitment to the lamina (Towbin et al., 2012). We noted a slight, but not statistically significant, loss of association of our targeting fragments but were struck by a qualitative difference in the lamina association.

Because of these conflicting studies in the literature and our somewhat ambiguous cytological data, we decided to repeat this experiment to enable both cytological and DamID analyses.

Specifically, we treated cells harboring relocated TCIS sites with BIX-01294 for 12 h and then transduced these cells with Dam or Dam-LMNB1 and harvested after 48 h (total of 60 h). We noted some slowdown of cell division at this time point, but the cells were healthy and still undergoing division (unpublished data; Kubicek et al., 2007). At this time point, there is statistically significant repositioning away from the nuclear lamina, but at a relatively low frequency (Fig. 8 D). However, by using DamID to measure lamina association, there was, quite strikingly, a complete
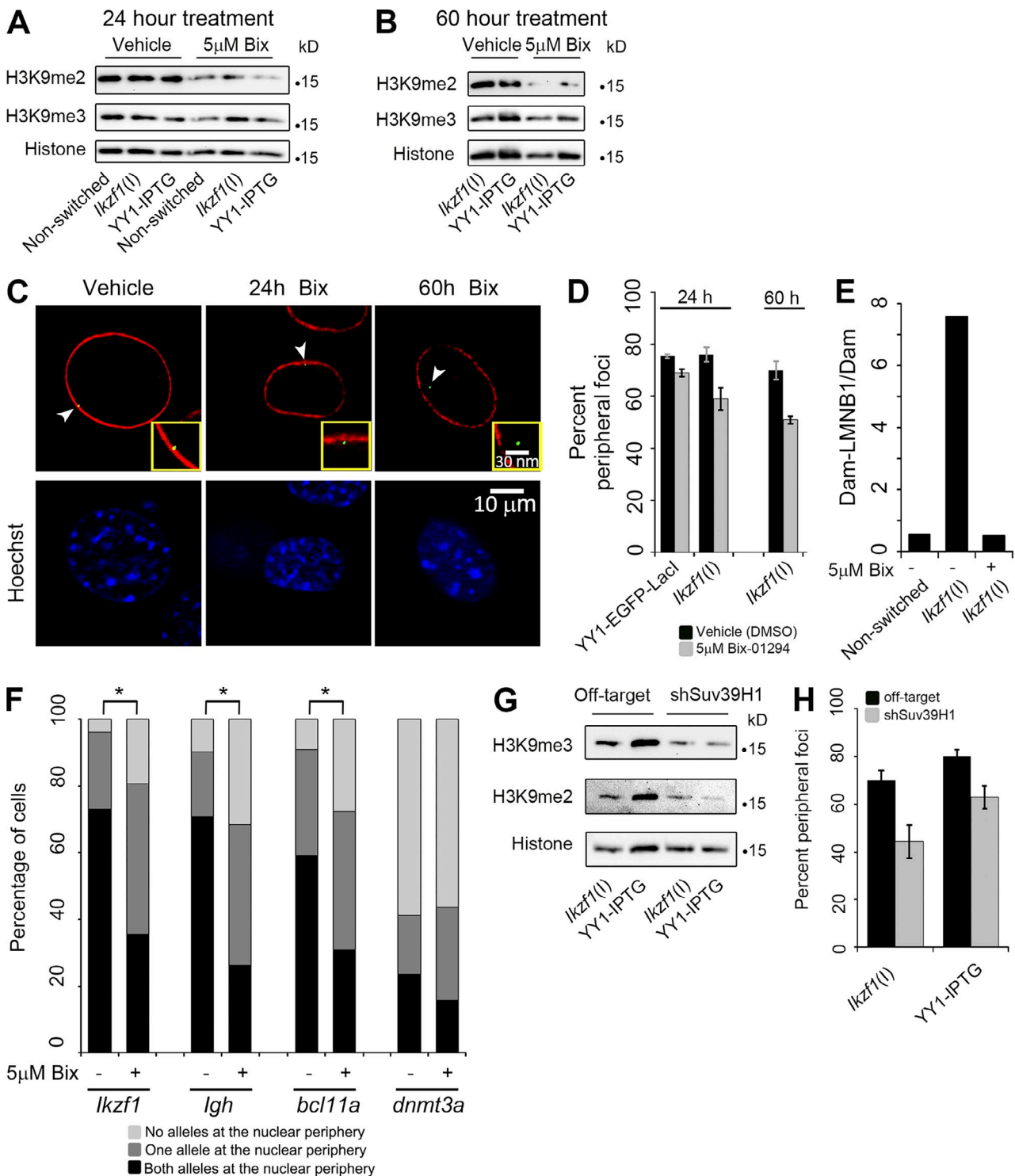
Figure 8. **H3K9me2/3 is necessary for de novo LAD formation.** (A and B) Immunoblot analysis of protein lysates from TCIS lines either harboring *Ikzf1 (I)* LAS or bound by YY1-EGFP-LacI (−IPTG) and nonswitched control. Cells were treated with either vehicle (DMSO) or 5 µM Bix-01294 for 24 or 60 h. Proteins were detected by the antibodies indicated; loading control is total histone H3. (C) Representative images of clone Y harboring the *Ikzf1 (I)* LAS ± 5 µM Bix-01294 after 24- or 60-h treatment. EGFP-LacI foci (arrowheads), LMNB1 (red), and Hoechst (blue) are shown. Insets are 300× magnifications. (D) Quantitation of the disposition of the TCIS insert for vehicle and 5 µM Bix-01294 treatment at 24- and 60-h treatment of clone Y harboring *Ikzf1 (I)* LAS and YY1-EGFP-LacI (−IPTG, *n* ≥ 50). (E) qPCR analysis of DamID in clone Y harboring *Ikzf1* (I) LAS ±5 µM Bix-01294 (60 h). A value >1, of Dam-LMNB1 over Dam only, indicates enrichment of the tested locus. Positive and negative controls are primers to an internal region of the *Igh* locus and a non–lamina-associated region, dip, as previously described. The data shown are from a single representative experiment. (F) Quantitation of 3D DNA immuno-FISH for the indicated proteins in 48-h, 5 µM Bix-01294–treated MEFs (*n* ≥ 50; *, P ≤ 0.01). (G) Immunoblot analysis of protein lysates from TCIS clone Y harboring *Ikzf1 (I)* LAS or YY1-EGFP-LacI (−IPTG) treated with the indicated shRNAs. Proteins were detected by the antibodies indicated; loading control is total histone H3. (H) Quantitation of the disposition of TCIS sites of clone Y harboring *Ikzf1 (I)* LAS or bound by YY1-EGFP-LacI–treated shRNAs as indicated (48 h, *n* ≥ 50). Error bars indicate SD.

Figure 9. **A model for directed reorganization of chromatin.** A cross section of a portion of the interior of an FB nucleus shows chromatin as a lamina-associated domain (LAD, red with yellow borders) or a non–lamina-associated region (green). An ectopic insertion of a LAS into the TCIS insert site is poised for relocation to the lamina caused by H3K9me2/3 modifications present on the insert (red). Acquisition of H3K27me3 (yellow) leads to lamina association. Abrogation of H3K27me3 by knockdown of EZH2 or specific transcriptional repressors or by drug inhibition leads to loss of peripheral targeting at both endogenous and ectopic loci. Our data suggest that K27me3 precedes movement to the lamina. Abrogation of H3K9me2/3 leads to a loss of association of endogenous and ectopic loci, as has also been shown by previous studies (Towbin et al., 2012; Bian et al., 2013; Kind et al., 2013). We propose that these two facultative heterochromatin marks, H3K27me3 and H3K9me2/3, cooperate (bivalently) to drive LAD formation and/or maintenance. Intriguingly, we also uncovered a potential role for LMNC (or LMNA/C levels) in this process, and disruptions in LMNA/C have been linked to global loss of H3K27me3 as well as H3K9me3 (Luperchio et al., 2014; Wong et al., 2014). ONM, outer nuclear membrane; INM, inner nuclear membrane.
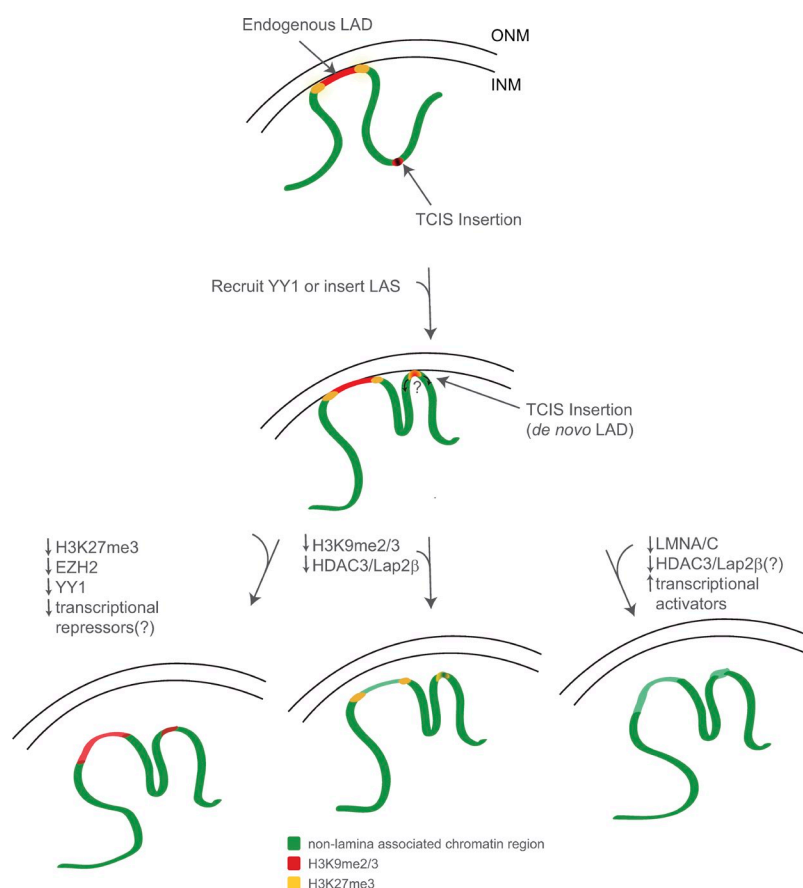
loss of association with the nuclear lamina (Fig. 8 E). We tested whether BIX-01294 treatment affected endogenous loci as well and chose to use an intermediate time point (48 h). The endogenous loci, in contrast to our TCIS relocated fragments, show appreciable loss of association (Fig. 8 F). We next queried whether H3K9me3 affected our loci in the same way by using an shRNA-mediated knockdown of the SUV39H1 (Suppressor of Variegation 3–9 homologue 1), a methyltransferase that mediates H3K9me3 (Fig. 8, G and H; Lachner and Jenuwein, 2002). Although SUV39H1 knockdown did disrupt localization of both the LAS- and YY1-directed lamina association, we were unable to attribute this directly to H3K9me3 because removal of SUV39H1 also perturbed H3K9me2 levels (Fig. 8 G). Although we found this result somewhat surprising, we note that loss of SUV39H1 has previously been shown to disrupt H3K9me2 (Murayama et al., 2008). Nonetheless, these data provide compelling evidence that both H3K27me3 and H3K9me2/3 are required for targeting an ectopic site to the nuclear lamina.

Discussion

Our results implicate specific DNA sequences within LADs and chromatin state, specifically H3K27me3 and H3K9me2/3, in establishing de novo lamina associations. In addition, we suggest a role for levels of A-type lamins and, specifically, LMNC in regulating this repositioning (Fig. 9). Our work focused on LAD border regions. We show that some LASs are sufficient for directing an ectopic site to the nuclear lamina, and this repositioning is

dependent on YY1 (Fig. 4) and H3K27me3 (Figs. 4 and 7), a histone modification demonstrated to be enriched in these regions at endogenous LADs (Figs. 6 and 3 A; Shah et al., 2013). We demonstrate, in agreement with two previous studies, that directed association with the nuclear lamina is also dependent on H3K9me2/3 (Fig. 8; Towbin et al., 2012; Bian et al., 2013). In addition, a recent study, using a human fibrosarcoma cancer cell line (HTC75), demonstrated that using either BIX-01294 or G9a shRNA-mediated knockdown to perturb H3K9me2 resulted in loss of LAD association with the nuclear periphery (Kind et al., 2013). Recent work in our laboratory also shows that these modifications are necessary for functional organization of a chromosomal territory (unpublished data). Thus, we speculate that these LAD border regions, which are enriched in both H3K27me3 and H3K9me2/3, constitute a targeting signal for LAD formation (Fig. 9). Intriguingly, recent studies have also identified specific nuclear envelope transmembrane proteins as involved in organizing and regulating chromatin at the nuclear periphery (Reddy et al., 2008; Zuleger et al., 2013; Wong et al., 2014). We therefore propose a model for regulation of vLADs that incorporates cell type–specific transcription factors, chromatin modifiers and organizers, and nuclear lamina proteins to facilitate cell type–specific genome organization (Fig. 9).

The work described herein focused on functional tests of LAD organization at LAD borders. In agreement with a previous study, we find that GA-rich sequence motifs, potentially bound by BTB-POZ domain proteins, are overrepresented in lamina relocating fragments but also find an enrichment of YY1 and

CTCF binding sites (Figs. 3 C and S4). The presence of CTCF binding sites was not unexpected as a result of its known enrichment at the boundaries of LADs (Vogel et al., 2007; Guelen et al., 2008; Handoko et al., 2011). As a previous study has indicated that robust YY1 binding often requires a cofactor (Golebiowski et al., 2012), we speculate that Zbtb7b or another transcription factor (or even CTCF) may be required to recruit or enhance YY1 or PRC2 binding in vLAD border sequences to facilitate repositioning to the lamina. In support of this, a recent study has implicated BTB-POZ domain proteins in the recruitment of PRC2 to chromatin, possibly through interactions with YY1 (Boulay et al., 2012). Intriguingly, in *Drosophila melanogaster* neurons, competition by BTB-POZ–related proteins for GAGA sites determines the disposition and transcription state of the neural competence factor *Hunchback* (Lehmann et al., 1998; Kohwi et al., 2013). It is therefore tempting to speculate that specific cell type–specific transcription factors can promote or inhibit association with the nuclear lamina through their interactions with chromatin remodelers for the induction of large scale chromatin changes concurrent with either localization to or away from the nuclear periphery. This latter point is important because transcriptional activation appears to disrupt associations with the nuclear lamina (Tumbar et al., 1999; Tumbar and Belmont, 2001; Bubulya and Spector, 2004). Both Zbtb7b and YY1 have been shown to repress and activate genes, adding to the potential for cell type–specific functionality of these proteins in scaffolding to the nuclear lamina.

There are studies in the literature indicating that YY1 may interact with and enhance the activity of HDAC3, thus potentially linking cell type–specific regulation through factors such as Zbtb7b, with a more general model implicating epigenome/genome organizers and specific structural proteins (e.g., LMNA/C and Lap2-β) at the nuclear periphery in positioning chromatin to the nuclear lamina (Fig. 9; Somech et al., 2005; Sankar et al., 2008; Faulk and Kim, 2009; Atchison, 2014; Luperchio et al., 2014). Interestingly, CTCF has been proposed to interact with YY1 to mediate cell type–specific organization, raising the possibility that CTCF and YY1 act together to target and delimit LAD boundaries (Phillips-Cremins et al., 2013). Numerous studies have implicated the interaction of these two proteins in both nuclear architecture and in gene regulation (Donohoe et al., 2007; Kim, 2008; Nikolaev et al., 2009; Degner et al., 2011; Weth and Renkawitz, 2011; Medvedovic et al., 2013; Wei et al., 2013).

Finally, our results also suggest that LMNA/C is important in instructing the peripheral localization of these sequences (Fig. 4). Two recent studies have implicated LMNA in large scale chromatin organization, but these data did not differentiate between LMNA and LMNC (McCord et al., 2013; Solovei et al., 2013). Our data suggest that either overall levels of LMNA/C are important or, more intriguingly, that LMNC is required for proper genome organization. What is clear from our results is that LMNA is not necessary for recruitment or retention at the nuclear lamina. This suggests, contrary to the commonly held position that there is functional redundancy between LMNA and C, that LMNC may be specifically involved in instructing peripheral positioning. Consistent with this, are studies that "LMNC-only" mice (missing LMNA but with normal LMNC

levels) are viable, yet LMNA/C$^{+/-}$ have perturbed differentiation (Fong et al., 2006; Sehgal et al., 2013). Intriguingly, we detect both H3K27me3 and YY1 at the nuclear lamina, especially in YY1-overexpressing cells. Given our overall results, it is tempting to speculate that YY1 and PRC2 interact with the lamina to facilitate both nuclear positioning and regulation of LADs.

Materials and methods

Identification of lamin association

MEFs were purchased from ATCC (CRL-2752) and cultured according to their establish protocols. *Rag2$^{-/-}$* pro–B cells were derived by isolating lineage-depleted hematopoietic cells from the bone marrow of B6 (Cg)-*Rag2tm1.1Cgn*/J (JAX catalog no. 008449; The Jackson Laboratory), which harbor a deletion of exon 3 in the coding region of the RAG2 gene. Isolation was followed by ex vivo differentiation and expansion on OP9 stromal cells initially with SCF and IL-7 and then IL-7 alone in OptiMEM media with 5% FBS. DamID was performed as described previously (Reddy et al., 2008; Zullo et al., 2012). In brief, self-inactivating retroviral constructs pSMGV Dam-V5 (Dam only) and pSMGV Dam-V5-LMNB1 (Dam-LMNB1) were used to generate retrovirus using the Platinum-E packaging cell line (RV-101; Cell Biolabs). Supernatants containing viral particles were collected between 48 and 72 h after transfection of the DamID constructs, and collection times were pooled. C57BL/6 MEFs were incubated overnight with either Dam-only or Dam-LMNB1 viral supernatant and 8 µg polybrene. Ex vivo expanded Rag2$^{-/-}$ pro–B cells were spinfected by centrifuging in 24- or 48-well plates at 500 *g* for 2 h with viral supernatant plus 3 ng/ml interleukin-7 (IL-7) and 4 µg polybrene at room temperature. After the spin, the cells were allowed to recover for 1 h at in a tissue culture incubator (5% CO$_2$, 37°C with humidity) before removing the viral supernatants and moving onto OP-9 stromal cells with normal growth medium (OptiMEM, 5% FBS, and 3 ng/ml IL-7). DamID was performed as previously described (Vogel et al., 2007; Zullo et al., 2012). In brief, DNA was isolated from cells expressing Dam or Dam-LMNB1 using DNA Mini kit (QIAGEN), precipitated, and resuspended to 1 µg/µl. 2 µg of this genomic DNA was digested overnight with the restriction enzyme DpnI (R0176L; New England Biolabs, Inc.), which cuts at methylated GA^{me}TC. After digestion, double-stranded adapters comprising annealed oligonucleotide *AdRt* (5′-CTAATACGACTCACTATAGGGCAGCGTGGTCGCGGCC-GAGGA-3′) and *AdRb* (5′-TCCTCGGCCG-3′) were ligated overnight with the digested DpnI fragments (T4 ligase 799009; Roche) followed by DPNII digestion (R0543S; New England Biolabs, Inc.) for 1 h. This material was amplified in ligation-mediated PCR using *AdR_PCR* primer (5′-GGTCGCG-GCCGAGGATC-3′) and Advantage cDNA Polymerase (Takara Bio Inc.). The resulting material was checked by agarose gel electrophoresis to ensure that specific amplification of methylated DNA fragments occurred and then column purified (QIAquick PCR purification kit; QIAGEN). This material was used either for qPCR assays or subjected to array hybridization. For qPCR assays, we used the following primer sets: specific to a region of the TCIS insert (*TCIS_ChIP_F1*, 5′-AGCTTGGCGTAATCATGGTC-3′, and *ChIP_R5*, 5′-ATTAGGCACCCCAGGCTTTA-3′), specific to an internal *Igh* LAD region (*J558_1*, 5′-AGTGCAGGGCTCACAGAAAA-3′, and *J558_12*, 5′-CAGCTCCATCCCATGGTTAGA-3′), or specific to a lamina-negative region in a LAD (also called Dip; *chr10:105245772_141bp_F*, 5′-AGGG-ACAGCCGTGGAGGAGC-3′, and *chr10:105245772_141bp_R*, 5′-CC-GCACCGTCCGGTTCTCAG-3′; Reddy et al., 2008). For identification of large genomic regions, Dam-only and Dam-LMNB1 samples were labeled with Cy3 and Cy5 using a random prime strategy, and DamID samples were hybridized to mouse whole genome tiling array 3 of 4 (mm8, part of chromosome 9 to part of chromosome 14; Economy Array; NimbleGen) using standard protocols. Arrays were scanned using a scanner (MS200_2), and probe intensity log$_2$ ratios Dam-LMNB1 to Dam only were obtained using DEVA 1.0.2 software (Roche NimbleGen). All experiments were performed two independent times. DamID array signal intensity data were lifted over to mm9 using the Galaxy converter tool, and then, data from replicate arrays were averaged together (Giardine et al., 2005; Blankenberg et al., 2010; Goecks et al., 2010). DamID data were quantile normalized and smoothed using the preprocessCore R package (Bolstad, 2003) and then segmented via a modified circular binary segmentation using the DNAcopy R package (Seshan and Olshen, 2014), which is an algorithm for identifying copy number difference, which "tests for change-points using a maximal *t*-statistic with a permutation reference distribution to obtain the

corresponding *P*-value" (Venkatraman and Olshen, 2007). A sliding window approach with a window size of 2 kb was used to combine neighboring segments, using in-house perl scripts. Code and accessory scripts are provided (supplemental material). Regions identified that were <25 kb were trimmed from total LAD data. LAD and non-LAD regions were identified across chromosomes 11 and 12. non-LAD regions were identified as the complementary regions to LADs via the complement function in Galaxy (GSE56990).

Analysis of LADs and genomic features
YY1, CTCF, and H3K27me3 ChIP data were tested for statistically significant overlap of LADs in FBs using the GenometriCorr package (Mendenhall et al., 2010; Peric-Hupkes et al., 2010; Favorov et al., 2012; Vella et al., 2012; Simon et al., 2013). The GenometriCorr package applies multiple spatial tests of independence including an absolute distance test (i.e., if two elements such as LADs and YY1 sites are a fixed distance from each other), projection test (i.e., testing for significant overlap between these two positions assuming they represent single points points), and the Jaccard test (testing for correlation of these two positions assuming that they are not points but instead occupy some interval of the genome). In addition to these statistical tests, the intensities of the DamID and ChIP peak data were plotted against bioinformatically determined LAD border regions (±50,000 kbp) to generate intensity profiles of the tested binding data for CTCF, YY1, H3K27me3, and LMNB1 using the Genomation R package (Akalin and Franke, 2014). 200 bins were generated over the entire border interval (±50,000 kbp), and signal intensities of binding data within each bin were averaged and plotted.

Motif identification
BAC-derived fragments DNA tested for repositioning effects were analyzed for known and de novo motifs, performed with MEME Suite and MotifSuite (Bailey et al., 2009; Claeys et al., 2012). Specifically, sequences from relocating fragments were analyzed using both MEME Suite (MEME [Multiple EM for Motif Elicitation]) using default parameters. Identified motifs were compared with the expected frequency in chromosome 11 background (because the tested fragments were from this chromosome), generated using the MotifSuite background generator tool CreateBackgroundModel. Enrichment of the targeting versus background and nonrelocating fragments was determined by using a 0.5 threshold parameter. Only motifs that displayed a twofold enrichment were considered for further evaluation. The identified motifs were then mapped to the fragments with the MAST program (Motif Alignment and Search Tool) in the MEME suite (Bailey and Gribskov, 1998). We then further confirmed the enrichment using randomly identified sequences in chromosome 11 away from LAD border regions and subjecting these to the same motif mapping via MAST. Only motifs identified as enriched over background on relocating fragments were further examined to identify proteins that may bind to these identified motifs using TomTom motif comparison software (Bailey et al., 2009).

BACs and fragments for positioning analysis
All BACs were obtained from the BACPAC Resource Center at Children's Hospital Oakland Research Institute (Oakland, CA). The listing of BACs with their NCBI clone IDs and the genes they contain is provided in Fig. S1 B. DNA fragments for analysis by random integration and switching analysis were created by sheering BAC DNA with a p200 tip 5–10 times. DNA was then run out on a 0.5% agarose gel, and DNA over 25 kb was isolated and cloned into a pcDNA3 vector. The pcDNA3 plasmids harboring BAC fragments were then isolated from these clones and screened for BAC DNA insert on an agarose gel. Clones containing fragments from 10 to 30 kb were sent as glycerol stocks to SeqWright Genomic Services (GE Healthcare) to sequence fragments of BACs from each end. Identified fragments were cloned between the inverted loxP sites of the switch vector, see Plasmids used for nuclear compartmentalization analysis. 2.5-kb fragments from the DNA fragments of *Ikzf1* fragment F from the vLAD near the gene *Ikzf1* were amplified from the fragments with the following primers: M24_D6_1_w, 5'-TGGGATAGTTCACAAGAAGCAC-3'; M24_D6_1_C, 5'-GTT-CATGCCTATGGCACAGC-3'; M24_D6_2_w, 5'-ACTTCATGCTGGGAGA-CAGG-3'; M24_D6_2_c, 5'-CTCTGCCTGTCCTGAAGCTC-3'; M24_D6_3_w, 5'-CCAGTGTGATGGTGCATACC-3'; M24_D6_3_c, 5'-GAGGGTG-TGTGTGTGTTTGG-3', M24_D6_4_w, 5'-ATCAACCAAGAGGCCAC-AAC-3'; M24_D6_4_c, 5'-AGAAGCCTCAGTCCATCGAG-3'; M24_D6_5_w, 5'-TTCCTGGTGCATCTGTGAAG-3'; M24_D6_5_c, 5'-CCTACGG-AGCCATTTTTCTG-3', M24_D6_6_w, 5'-CAGAAAAATGGCTCCGTAGG-3', M24_D6_6_c, 5'-ACAGGAGCTGGAGTGGTGAC-3', M24_D6_7_w, 5'-ACTTCAACCCCCACTTTTCC-3', M24_D6_7_c, 5'-AGGGAGGCCTTA-GAGCTGAC-3', M24_D6_8_w, 5'-GCAGAGTGGAAGCAAGGAAG-3';

M24_D6_8_c, 5'-ACCAGGGTGACCTTGAACTC-3'; M24_D6_9_w, 5'-TAAGGTGGCTGGAGAGATGG-3'; and M24_D6_9_c, 5'-TTTTGCA-GATTTCCCCTTTG-3'.

Plasmids used for nuclear compartmentalization analysis
The TCIS vector was constructed by flanking a hygromycin phosphotransferase-thymidine kinase gene (*HYTK*) with inverted LoxP sites. Subsequently, a 256-repeat *lacO* array was integrated upstream of the LoxP site. DNA fragments (see BACs and fragments for positioning analysis), for recombination, were cloned into a switch vector, the original recombination-mediated cassette exchange vector L1HYTK1L (Feng et al., 1999) was digested with BamHI to remove the cytomegalovirus promoter and hygromycin/thymidine kinase cassette, and the resulting fragment containing the inverted loxP sites was end polished (NEBNext End Repair Module; New England Biolabs, Inc.). Into this, we cloned a HincII–EcolRCI fragment containing the multiple cloning site from pBlueScript (pBS KS+). Cre recombinase was introduced by cotransfection with plasmid 24593 and AAV-pgk-cre obtained from Addgene (GenBank accession no. AY056050). The EGFP-LacI retroviral vector was made by ligating a DraI fragment containing GFP-LacI from p3′ssEGFP-LacI into an HpaI site in pMSCV-puro (Takara Bio Inc.). YY1-EGFP-LacI fusion proteins were generated by ligating YY1 (plasmid MC208051 mouse cDNA digested with SalI and PspXI; OriGene) upstream and in frame with EGFP-LacI in a retroviral vector (p3′ssEGFP-LacI, digested with SalI and PspXI). Zbtb7b-EGFP-LacI fusion protein was generated by ligating Zbtb7b (plasmid ZBTB7B in pANT7_cGST; clone ID FLH264179.01L [DNASU], digested with AvrII and PspXI upstream and in frame with EGFP-LacI in a retroviral vector (p3′ssEGFP-LacI, digested with SalI and PspXI).

Generation and propagation of C57BL/6 FB cell lines and clones
NIH3T3-derived C57BL/6 murine FBs (CRL-2752; ATCC) were transduced with the EGFP-LacI retroviral vector and selected with 1 µg/ml puromycin to generate a line expressing EGFP-LacI. Random integration clones were generated by transfecting the C57BL/6 EGFP-LacI lines with linearized BACs and hygromycin-selectable *lacO* arrays. TCIS cell lines were generated by transfecting C57BL/6 FB with a linearized TCIS construct described in Plasmids used for nuclear compartmentalization analysis. Cells were selected for hygromycin resistance (500 µg/ml), and clones were isolated and expanded. Single integration clones were screened for by qPCR and transfection with EGFP-LacI retroviral vector to visualize the insert site. Clones 12 and Y had single integrations of the TCIS system at a chromosomal position away from the nuclear lamina, as determined by microscopy and either the presence or lack of an overlap in LMNB1 and EGFP-LacI accumulation at the *lacO* insert site. Transfections for TCIS line establishment and random integrations were performed with FuGENE 6 (Promega). Site-specific recombination was obtained by cotransfection of TCIS clones with DNA fragments cloned into a switch vector and Cre recombinase. Switched cells were then seeded at low density with 10,000 cells per well of a 6-well tissue culture dish and treated with 1 µM ganciclovir for 24 h. TCIS cells require a short treatment with ganciclovir and to be treated at low confluence. Negative ganciclovir selection occurs when the nonswitched thymidine kinase gene cassette expresses thymidine kinase, which in turn phosphorylates ganciclovir. Phosphorylated ganciclovir is toxic to the cells. Once released into the media, it can affect neighboring cells if not maintained at low confluence and if media is removed after 24 h. Cells that have successfully switched cannot phosphorylate ganciclovir and are therefore resistant. Cells resistant to ganciclovir (1 µM) were then expanded for nuclear positioning analysis. Transfections for specific recombination in TCIS clones were performed with the electroporation system (Amaxa Nucleofector 4; Lonza), to ensure essentially 100% transfection efficiency. Ingenio Electroporation Products (MIR 50111; Mirus Bio LLC) were used in combination with the Amaxa nucleofector. All cell lines were maintained in DMEM high with 10% FBS (U.S. Defined Fetal Bovine Serum; Hyclone) in the presence of 500 µg/ml hygromycin (50 mg/ml; Hygromycin B; Corning/CellGro) and 1 mM IPTG when EGFP-LacI was present. To enable binding of EGFP-LacI, IPTG was removed from the cultures, and cells were analyzed after 24–36 h in fresh media. YY1- and Zbtb7b-EGFP-LacI–harboring cones were created by transduction of TCIS clones Y and 12 with the retroviral vector and selection with 1 µg/ml puromycin.

shRNA knockdowns and drug treatments
shLMNA was produced in our laboratory. shRNA-mediated knockdowns were performed by infecting FB clones with freshly produced lentivirus for the specific shRNA. Lentivirus was produced by cotransfecting the desired knockdown construct, Delta 8.9, and vsv-g vector into HEK293

cells. Virus was added to FB cells at ~30–40% confluence and removed after 12–14 h. New media were added to cells, and they were assayed 4 d after infection. shRNA constructs were obtained from Sigma-Aldrich (Mission shRNA database): shZbtb7b, clone NM_009565.4-2183s21c1; shYY1, clone NM_009537.2-918s1c; shCTCF, clone NM_007794.1-1030s1c1; shEZH2, clone NM_007971.2-421s21c1; shLMNA/C, clone NM_001002011.2-901s21c; and shSuv39H1, clone NM_011514.1-1874s1c1. Off-target controls were shRNA directed against firefly luciferase (5′-CGCTGAGTACTTCGAAATGTC-3′; a gift from the laboratory of D. Raben, Johns Hopkins University School of Medicine, Baltimore, MD). For G9a inhibition, MEFs and TCIS clone lines were treated with 5 µM Bix01294 for 24, 48, or 60 h as indicated. To reduce H3K27me3, MEFs and TCIS clones were treated with 5 µM DZNep for 24 h.

IF and 3D DNA immuno-FISH

Cells were prepared for IF by platting on sterilized 25-mm round coverslips (German borosilicate glass #1.5; Harvard Apparatus) in 6-well tissue culture dishes. The nuclear lamina was visualized using an anti-LMNB antibody (sc-6217, goat IgG; Santa Cruz Biotechnology, Inc.). IF coupled with DNA in situ hybridization on preserved nuclei (3D DNA immuno-FISH) was performed as previously described (Reddy et al., 2008). DNA hybridization probes were generated by nick translation in the presence of digoxigenin or biotin-conjugated nucleotides (DIG Nick Translation kit and Biotin Nick Translation kit; Roche). After probe hybridization, an anti-LMNB antibody was used to mark the nuclear lamina. Other antibodies used were histone H3 (1:1,000; sc-10809, rabbit IgG; Santa Cruz Biotechnology, Inc.), GFP (1:1,000; sc-8334, rabbit IgG; Santa Cruz Biotechnology, Inc.), H3K27me3 (1:1,000; 39155, rabbit IgG; Active Motif), H3K9me2 (1:200; ab1220, mouse IgG; Abcam), H3K9me3 (1:500; ab8898, rabbit IgG; Abcam), Zbtb7b (1:500; ab20985, rabbit IgG; Abcam), LMNA/C (1:500; sc-20681, rabbit IgG; Santa Cruz Biotechnology, Inc.), LMNA (1:500; sc-6214, goat IgG; Santa Cruz Biotechnology, Inc.), LacI (1:500; 05–503, mouse IgG1, Upstate Biologicals), YY1 (1:500; sc-7341, mouse IgG1; Santa Cruz Biotechnology, Inc.), CTCF (1:500; ab128873, rabbit IgG; Abcam), and β-actin (1:5,000; A5441, mouse IgG1, Sigma-Aldrich).

ChIP and qPCR

ChIP was performed as previously described (Reddy et al., 2008). In brief, cells were fixed in 0.5% formaldehyde for 15 min and then quenched with saturating amounts of glycine. Fixed cells were lysed in cell lysis buffer containing protease inhibitors (10 mM Tris-Cl, pH 8.1, 10 mM NaCl, and 0.5% NP-40) for 10 min, and the nuclei were then pelleted by centrifugation. Nuclei were resuspended in nuclei lysis buffer containing protease inhibitors (50 mM Tris-Cl, pH 8.1, 10 mM EDTA, and 1% SDS) for ≤10 min to generate the chromatin fraction. This chromatin was sonicated to a mean length of 600 base pairs and immunoprecipitated with 2.5–5 µg of the histone modification–specific or control antibody (antibodies: H3K27me3 [39155, rabbit IgG], H3K9me2 [ab1220, mouse IgG], and H3K9me3 [ab8898, rabbit IgG]). qPCR was performed using *Igh* primers specific for a region in the center of the locus (distal V gene region) as indicated in Fig. S5 and described previously (J558 10, 5′-AGTGCAGGGCT-CACAGAAAA-3′; and J558 12, 5′-CAGCTCCATCCCATGGTTAGA-3′; Reddy et al., 2008). Primers to test the chromatin state of TCIS insertions were specific to a region of the TCIS insert (TCIS_ChIP_F1, 5′-AGCTTGGC-GTAATCATGGTC-3′, and ChIP_R5, 5′-ATTAGGCACCCCAGGCTTTA-3′). Control primers were Acta2 up, 5′-CAGAGGAATGCAGTGGAAGAGAC-3′, and Acta2 down, 5′-TCGCTTCCCAAACAAGGAGC-3′.

Image acquisition and preparation details

All Imaging was performed on an inverted fluorescence microscope (Axio-Vision; Carl Zeiss) fitted with an ApoTome and camera (AxioCam MRm; Carl Zeiss). The objective lens used was a 100× Apochromat oil immersion (Carl Zeiss) with an NA of 1.5 (Immersol 518; Carl Zeiss). All IF was performed at room temperature on #1.5 coverslips. 3D DNA immuno-FISH experiments were either performed on #1.5 coverslips or on slides and mounted with #1.5 coverslips. All IF and 3D DNA immuno-FISH samples were mounted in either VECTASHIELD (Vector Laboratories) or SlowFade gold (Life Technologies). AxioVision software (Carl Zeiss) was used for image acquisition. Images were exported as TIFFs to ImageJ (National Institutes of Health) for further analyses. EGFP-LacI/*lacO* foci were scored as either overlapping with lamin signal (LMNB, peripheral) or not coincident with lamina (central). Images were adjusted using only brightness and contrast. When comparing expression levels, experiments were performed in parallel, imaged at the same exposure times, and adjusted in parallel

to show differences in protein expression. Each experiment was prepared in duplicate and scored as either peripheral or not peripheral by two different people, one of which was blind to the experimental conditions. The data analyzed by these two individuals were compared to ensure accurate measurements. SD was then calculated on the mean scores from these two observers on two independent experiments for each observation ($n = 2$, SD refers to SD between experiments). Only data collected by one of the individuals were included for determination of p-values to avoid aberrantly inflating the observed n. P-values for each experiment and condition were calculated by first converting our scored data into either peripheral (1) or not peripheral (0). The distributions of this converted data from a control experiment were compared with the treated/experimental data using an unpaired t test.

Online supplemental material

Fig. S1 shows a wide-scale view of LADs as determined by Dam-LMNB1 relative to the background control, Dam only, in multiple cell types. Fig. S2 shows random integration experiments of all regions of interest and additional directed recombination of sequences from the FB-specific vLAD-containing Bcl11a. Fig. S3 shows a schematic of the TCIS system along with data to validate its presence and functionality in our FB TCIS clone lines. Fig. S4 characterizes positioning by small LAS fragments at the edge of a LAD border and shows how potential protein candidates were identified for further functional analyses. Fig. S5 shows cell viability for all knockdown and drug treatment experiments, as well as the nuclear location and distribution of endogenous and overexpressed YY1 in FBs, and that directed recruitment of YY1 is not to pericentric heterochromatin. A ZIP file is also provided that includes code and accessory scripts. Online supplemental material is available at http://www.jcb.org/cgi/content/full/jcb.201405110/DC1.

References

Akalin, A., and V. Franke. 2014. Genomation—a toolkit for annotation and visualization of genomic data. http://bioinformatics.mdc-berlin.de/genomation/ (accessed December 9, 2014).

Atchison, L., A. Ghias, F. Wilkinson, N. Bonini, and M.L. Atchison. 2003. Transcription factor YY1 functions as a PcG protein in vivo. *EMBO J.* 22:1347–1358. http://dx.doi.org/10.1093/emboj/cdg124

Atchison, M.L. 2014. Function of YY1 in long-distance DNA interactions. *Front. Immunol.* 5:45. http://dx.doi.org/10.3389/fimmu.2014.00045

Bailey, T.L., and M. Gribskov. 1998. Combining evidence using p-values: application to sequence homology searches. *Bioinformatics*. 14:48–54. http://dx.doi.org/10.1093/bioinformatics/14.1.48

Bailey, T.L., M. Boden, F.A. Buske, M. Frith, C.E. Grant, L. Clementi, J. Ren, W.W. Li, and W.S. Noble. 2009. MEME SUITE: tools for motif discovery and searching. *Nucleic Acids Res.* 37(Web Server):W202–W208. http://dx.doi.org/10.1093/nar/gkp335

Basu, A., and M.L. Atchison. 2010. CtBP levels control intergenic transcripts, PHO/YY1 DNA binding, and PcG recruitment to DNA. *J. Cell. Biochem.* 110:62–69.

Basu, A., F.H. Wilkinson, K. Colavita, C. Fennelly, and M.L. Atchison. 2014. YY1 DNA binding and interaction with YAF2 is essential for Polycomb recruitment. *Nucleic Acids Res.* 42:2208–2223. http://dx.doi.org/10.1093/nar/gkt1187

Belmont, A.S., G. Li, G. Sudlow, and C. Robinett. 1999. Visualization of large-scale chromatin structure and dynamics using the lac operator/lac repressor reporter system. *Methods Cell Biol.* 58:203–222. http://dx.doi.org/10.1016/S0091-679X(08)61957-3

Bian, Q., N. Khanna, J. Alvikas, and A.S. Belmont. 2013. β-Globin cis-elements determine differential nuclear targeting through epigenetic modifications. *J. Cell Biol.* 203:767–783. http://dx.doi.org/10.1083/jcb.201305027

Blankenberg, D., G. Von Kuster, N. Coraor, G. Ananda, M. Lazarus, M. Mangan, A. Nekrutenko, and J. Taylor. 2010. Galaxy: a web-based genome analysis tool for experimentalists. *Curr. Protoc. Mol. Biol.* Chapter 19:Unit 19.10.1–19.10.21.

Bolstad, B.M. 2003. preprocessCore: A collection of pre-processing functions. R package version 1.26.1. http://www.bioconductor.org/packages/release/bioc/html/preprocessCore.html (accessed December 9, 2014).

Boulay, G., M. Dubuissez, C. Van Rechem, A. Forget, K. Helin, O. Ayrault, and D. Leprince. 2012. Hypermethylated in cancer 1 (HIC1) recruits polycomb repressive complex 2 (PRC2) to a subset of its target genes through interaction with human polycomb-like (hPCL) proteins. *J. Biol. Chem.* 287:10509–10524. http://dx.doi.org/10.1074/jbc.M111.320234

Bubulya, P.A., and D.L. Spector. 2004. "On the move"ments of nuclear components in living cells. *Exp. Cell Res.* 296:4–11. http://dx.doi.org/10.1016/j.yexcr.2004.03.018

Caretti, G., M. Di Padova, B. Micales, G.E. Lyons, and V. Sartorelli. 2004. The Polycomb Ezh2 methyltransferase regulates muscle gene expression and skeletal muscle differentiation. *Genes Dev.* 18:2627–2638. http://dx.doi.org/10.1101/gad.1241904

Claeys, M., V. Storms, H. Sun, T. Michoel, and K. Marchal. 2012. MotifSuite: workflow for probabilistic motif detection and assessment. *Bioinformatics.* 28:1931–1932. http://dx.doi.org/10.1093/bioinformatics/bts293

Cole, E.G., and K. Gaston. 1997. A functional YY1 binding site is necessary and sufficient to activate Surf-1 promoter activity in response to serum growth factors. *Nucleic Acids Res.* 25:3705–3711. http://dx.doi.org/10.1093/nar/25.18.3705

Cremer, M., J. von Hase, T. Volm, A. Brero, G. Kreth, J. Walter, C. Fischer, I. Solovei, C. Cremer, and T. Cremer. 2001. Non-random radial higher-order chromatin arrangements in nuclei of diploid human cells. *Chromosome Res.* 9:541–567. http://dx.doi.org/10.1023/A:1012495201697

Cremer, T., M. Cremer, S. Dietzel, S. Müller, I. Solovei, and S. Fakan. 2006. Chromosome territories—a functional nuclear landscape. *Curr. Opin. Cell Biol.* 18:307–316. http://dx.doi.org/10.1016/j.ceb.2006.04.007

Degner, S.C., J. Verma-Gaur, T.P. Wong, C. Bossen, G.M. Iverson, A. Torkamani, C. Vettermann, Y.C. Lin, Z. Ju, D. Schulz, et al. 2011. CCCTC-binding factor (CTCF) and cohesin influence the genomic architecture of the Igh locus and antisense transcription in pro-B cells. *Proc. Natl. Acad. Sci. USA.* 108:9566–9571. http://dx.doi.org/10.1073/pnas.1019391108

Donohoe, M.E., L.-F. Zhang, N. Xu, Y. Shi, and J.T. Lee. 2007. Identification of a Ctcf cofactor, Yy1, for the X chromosome binary switch. *Mol. Cell.* 25:43–56. http://dx.doi.org/10.1016/j.molcel.2006.11.017

Elcock, L.S., and J.M. Bridger. 2010. Exploring the relationship between interphase gene positioning, transcriptional regulation and the nuclear matrix. *Biochem. Soc. Trans.* 38:263–267. http://dx.doi.org/10.1042/BST0380263

Faulk, C.D., and J. Kim. 2009. YY1's DNA-binding motifs in mammalian olfactory receptor genes. *BMC Genomics.* 10:576. http://dx.doi.org/10.1186/1471-2164-10-576

Favorov, A., L. Mularoni, L.M. Cope, Y. Medvedeva, A.A. Mironov, V.J. Makeev, and S.J. Wheelan. 2012. Exploring massive, genome scale datasets with the GenometriCorr package. *PLOS Comput. Biol.* 8:e1002529. http://dx.doi.org/10.1371/journal.pcbi.1002529

Fedorova, E., and D. Zink. 2008. Nuclear architecture and gene regulation. *Biochim. Biophys. Acta.* 1783:2174–2184. http://dx.doi.org/10.1016/j.bbamcr.2008.07.018

Feng, Y.Q., J. Seibler, R. Alami, A. Eisen, K.A. Westerman, P. Leboulch, S. Fiering, and E.E. Bouhassira. 1999. Site-specific chromosomal integration in mammalian cells: highly efficient CRE recombinase-mediated cassette exchange. *J. Mol. Biol.* 292:779–785. http://dx.doi.org/10.1006/jmbi.1999.3113

Ferrai, C., I.J. de Castro, L. Lavitas, M. Chotalia, and A. Pombo. 2010. Gene positioning. *Cold Spring Harb. Perspect. Biol.* 2:a000588. http://dx.doi.org/10.1101/cshperspect.a000588

Finlan, L.E., D. Sproul, I. Thomson, S. Boyle, E. Kerr, P. Perry, B. Ylstra, J.R. Chubb, and W.A. Bickmore. 2008. Recruitment to the nuclear periphery can alter expression of genes in human cells. *PLoS Genet.* 4:e1000039. http://dx.doi.org/10.1371/journal.pgen.1000039

Fiskus, W., Y. Wang, A. Sreekumar, K.M. Buckley, H. Shi, A. Jillella, C. Ustun, R. Rao, P. Fernandez, J. Chen, et al. 2009. Combined epigenetic therapy with the histone methyltransferase EZH2 inhibitor 3-deazaneplanocin A and the histone deacetylase inhibitor panobinostat against human AML cells. *Blood.* 114:2733–2743. http://dx.doi.org/10.1182/blood-2009-03-213496

Fong, L.G., J.K. Ng, J. Lammerding, T.A. Vickers, M. Meta, N. Coté, B. Gavino, X. Qiao, S.Y. Chang, S.R. Young, et al. 2006. Prelamin A and lamin A appear to be dispensable in the nuclear lamina. *J. Clin. Invest.* 116:743–752. http://dx.doi.org/10.1172/JCI27125

Giardine, B., C. Riemer, R.C. Hardison, R. Burhans, L. Elnitski, P. Shah, Y. Zhang, D. Blankenberg, I. Albert, J. Taylor, et al. 2005. Galaxy: a platform for interactive large-scale genome analysis. *Genome Res.* 15:1451–1455. http://dx.doi.org/10.1101/gr.4086505

Goecks, J., A. Nekrutenko, and J. Taylor; Galaxy Team. 2010. Galaxy: a comprehensive approach for supporting accessible, reproducible, and transparent computational research in the life sciences. *Genome Biol.* 11:R86. http://dx.doi.org/10.1186/gb-2010-11-8-r86

Golebiowski, F.M., A. Górecki, P. Bonarek, M. Rapala-Kozik, A. Kozik, and M. Dziedzicka-Wasylewska. 2012. An investigation of the affinities, specificity and kinetics involved in the interaction between the Yin Yang 1 transcription factor and DNA. *FEBS J.* 279:3147–3158. http://dx.doi.org/10.1111/j.1742-4658.2012.08693.x

Guelen, L., L. Pagie, E. Brasset, W. Meuleman, M.B. Faza, W. Talhout, B.H. Eussen, A. de Klein, L. Wessels, W. de Laat, and B. van Steensel. 2008. Domain organization of human chromosomes revealed by mapping of nuclear lamina interactions. *Nature.* 453:948–951. http://dx.doi.org/10.1038/nature06947

Handoko, L., H. Xu, G. Li, C.Y. Ngan, E. Chew, M. Schnapp, C.W. Lee, C. Ye, J.L. Ping, F. Mulawadi, et al. 2011. CTCF-mediated functional chromatin interactome in pluripotent cells. *Nat. Genet.* 43:630–638. http://dx.doi.org/10.1038/ng.857

Heydarian, M., T.R. Luperchipo, J. Cutler, C.J. Mitchell, M.-S. Kim, A. Pandey, B. Sollner-Webb, and K. Reddy. 2014. Prediction of gene activity in early B cell development based on an integrative multi-omics analysis. *J. Proteomics Bioinform.* 7:50–63. http://dx.doi.org/10.4172/jpb.1000302

Janicki, S.M., T. Tsukamoto, S.E. Salghetti, W.P. Tansey, R. Sachidanandam, K.V. Prasanth, T. Ried, Y. Shav-Tal, E. Bertrand, R.H. Singer, and D.L. Spector. 2004. From silencing to gene expression: real-time analysis in single cells. *Cell.* 116:683–698. http://dx.doi.org/10.1016/S0092-8674(04)00171-0

Johnson, K., D.L. Pflugh, D. Yu, D.G.T. Hesslein, K.-I. Lin, A.L.M. Bothwell, A. Thomas-Tikhonenko, D.G. Schatz, and K. Calame. 2004. B cell-specific loss of histone 3 lysine 9 methylation in the V(H) locus depends on Pax5. *Nat. Immunol.* 5:853–861. http://dx.doi.org/10.1038/ni1099

Johnson, K., T. Hashimshony, C.M. Sawai, J.M. Pongubala, J.A. Skok, I. Aifantis, and H. Singh. 2008. Regulation of immunoglobulin light-chain recombination by the transcription factor IRF-4 and the attenuation of interleukin-7 signaling. *Immunity.* 28:335–345. http://dx.doi.org/10.1016/j.immuni.2007.12.019

Johnson, K., K.L. Reddy, and H. Singh. 2009. Molecular pathways and mechanisms regulating the recombination of immunoglobulin genes during B-lymphocyte development. *Adv. Exp. Med. Biol.* 650:133–147. http://dx.doi.org/10.1007/978-1-4419-0296-2_11

Josse, T., H. Mokrani-Benhelli, R. Benferhat, E. Shestakova, Z. Mansuroglu, H. Kakanakou, A. Billecocq, M. Bouloy, and E. Bonnefoy. 2012. Association of the interferon-β gene with pericentromeric heterochromatin is dynamically regulated during virus infection through a YY1-dependent mechanism. *Nucleic Acids Res.* 40:4396–4411. http://dx.doi.org/10.1093/nar/gks050

Kim, J. 2008. Multiple YY1 and CTCF binding sites in imprinting control regions. *Epigenetics.* 3:115–118. http://dx.doi.org/10.4161/epi.3.3.6176

Kind, J., L. Pagie, H. Ortabozkoyun, S. Boyle, S.S. de Vries, H. Janssen, M. Amendola, L.D. Nolen, W.A. Bickmore, and B. van Steensel. 2013. Single-cell dynamics of genome-nuclear lamina interactions. *Cell.* 153:178–192. http://dx.doi.org/10.1016/j.cell.2013.02.028

Kohwi, M., J.R. Lupton, S.-L. Lai, M.R. Miller, and C.Q. Doe. 2013. Developmentally regulated subnuclear genome reorganization restricts neural progenitor competence in *Drosophila. Cell.* 152:97–108. http://dx.doi.org/10.1016/j.cell.2012.11.049

Kosak, S.T., J.A. Skok, K.L. Medina, R. Riblet, M.M. Le Beau, A.G. Fisher, and H. Singh. 2002. Subnuclear compartmentalization of immunoglobulin loci during lymphocyte development. *Science.* 296:158–162. http://dx.doi.org/10.1126/science.1068768

Kubicek, S., R.J. O'Sullivan, E.M. August, E.R. Hickey, Q. Zhang, M.L. Teodoro, S. Rea, K. Mechtler, J.A. Kowalski, C.A. Homon, et al. 2007. Reversal of H3K9me2 by a small-molecule inhibitor for the G9a histone methyltransferase. *Mol. Cell.* 25:473–481. http://dx.doi.org/10.1016/j.molcel.2007.01.017

Lachner, M., and T. Jenuwein. 2002. The many faces of histone lysine methylation. *Curr. Opin. Cell Biol.* 14:286–298. http://dx.doi.org/10.1016/S0955-0674(02)00335-6

Lee, J.-K., and K.-C. Kim. 2013. DZNep, inhibitor of S-adenosylhomocysteine hydrolase, down-regulates expression of SETDB1 H3K9me3 HMTase in human lung cancer cells. *Biochem. Biophys. Res. Commun.* 438:647–652. http://dx.doi.org/10.1016/j.bbrc.2013.07.128

Lehmann, M., T. Siegmund, K.G. Lintermann, and G. Korge. 1998. The pipsqueak protein of *Drosophila melanogaster* binds to GAGA sequences through a novel DNA-binding domain. *J. Biol. Chem.* 273:28504–28509. http://dx.doi.org/10.1074/jbc.273.43.28504

Lin, Y.C., C. Benner, R. Mansson, S. Heinz, K. Miyazaki, M. Miyazaki, V. Chandra, C. Bossen, C.K. Glass, and C. Murre. 2012. Global changes in the nuclear positioning of genes and intra- and interdomain genomic

interactions that orchestrate B cell fate. *Nat. Immunol.* 13:1196–1204. http://dx.doi.org/10.1038/ni.2432

Liu, H., M. Schmidt-Supprian, Y. Shi, E. Hobeika, N. Barteneva, H. Jumaa, R. Pelanda, M. Reth, J. Skok, K. Rajewsky, and Y. Shi. 2007. Yin Yang 1 is a critical regulator of B-cell development. *Genes Dev.* 21:1179–1189. http://dx.doi.org/10.1101/gad.1529307

Luperchio, T.R., X. Wong, and K.L. Reddy. 2014. Genome regulation at the peripheral zone: lamina associated domains in development and disease. *Curr. Opin. Genet. Dev.* 25:50–61. http://dx.doi.org/10.1016/j.gde.2013.11.021

Mathelier, A., X. Zhao, A.W. Zhang, F. Parcy, R. Worsley-Hunt, D.J. Arenillas, S. Buchman, C.Y. Chen, A. Chou, H. Ienasescu, et al. 2014. JASPAR 2014: an extensively expanded and updated open-access database of transcription factor binding profiles. *Nucleic Acids Res.* 42(D1):D142–D147. http://dx.doi.org/10.1093/nar/gkt997

McCord, R.P., A. Nazario-Toole, H. Zhang, P.S. Chines, Y. Zhan, M.R. Erdos, F.S. Collins, J. Dekker, and K. Cao. 2013. Correlated alterations in genome organization, histone methylation, and DNA-lamin A/C interactions in Hutchinson-Gilford progeria syndrome. *Genome Res.* 23:260–269. http://dx.doi.org/10.1101/gr.138032.112

Medina, K.L., and H. Singh. 2005. Gene regulatory networks orchestrating B cell fate specification, commitment, and differentiation. *Curr. Top. Microbiol. Immunol.* 290:1–14.

Medvedovic, J., A. Ebert, H. Tagoh, I.M. Tamir, T.A. Schwickert, M. Novatchkova, Q. Sun, P.J. Huis In 't Veld, C. Guo, H.S. Yoon, et al. 2013. Flexible long-range loops in the VH gene region of the Igh locus facilitate the generation of a diverse antibody repertoire. *Immunity*. 39:229–244. http://dx.doi.org/10.1016/j.immuni.2013.08.011

Meister, P., B.D. Towbin, B.L. Pike, A. Ponti, and S.M. Gasser. 2010. The spatial dynamics of tissue-specific promoters during *C. elegans* development. *Genes Dev.* 24:766–782. http://dx.doi.org/10.1101/gad.559610

Mendenhall, E.M., R.P. Koche, T. Truong, V.W. Zhou, B. Issac, A.S. Chi, M. Ku, and B.E. Bernstein. 2010. GC-rich sequence elements recruit PRC2 in mammalian ES cells. *PLoS Genet.* 6:e1001244. http://dx.doi.org/10.1371/journal.pgen.1001244

Meuleman, W., D. Peric-Hupkes, J. Kind, J.-B.B. Beaudry, L. Pagie, M. Kellis, M. Reinders, L. Wessels, and B. van Steensel. 2013. Constitutive nuclear lamina-genome interactions are highly conserved and associated with A/T-rich sequence. *Genome Res.* 23:270–280. http://dx.doi.org/10.1101/gr.141028.112

Miranda, T.B., C.C. Cortez, C.B. Yoo, G. Liang, M. Abe, T.K. Kelly, V.E. Marquez, and P.A. Jones. 2009. DZNep is a global histone methylation inhibitor that reactivates developmental genes not silenced by DNA methylation. *Mol. Cancer Ther.* 8:1579–1588. http://dx.doi.org/10.1158/1535-7163.MCT-09-0013

Misteli, T. 2005. Concepts in nuclear architecture. *BioEssays*. 27:477–487. http://dx.doi.org/10.1002/bies.20226

Murayama, A., K. Ohmori, A. Fujimura, H. Minami, K. Yasuzawa-Tanaka, T. Kuroda, S. Oie, H. Daitoku, M. Okuwaki, K. Nagata, et al. 2008. Epigenetic control of rDNA loci in response to intracellular energy status. *Cell*. 133:627–639. http://dx.doi.org/10.1016/j.cell.2008.03.030

Nikolaev, L.G., S.B. Akopov, D.A. Didych, and E.D. Sverdlov. 2009. Vertebrate protein CTCF and its multiple roles in a large-scale regulation of genome activity. *Curr. Genomics*. 10:294–302. http://dx.doi.org/10.2174/138920209788921038

O'Meara, M.M., and J.A. Simon. 2012. Inner workings and regulatory inputs that control Polycomb repressive complex 2. *Chromosoma*. 121:221–234. http://dx.doi.org/10.1007/s00412-012-0361-1

Pan, X., M. Papasani, Y. Hao, M. Calamito, F. Wei, W.J. Quinn Iii, A. Basu, J. Wang, S. Hodawadekar, K. Zaprazna, et al. 2013. YY1 controls Igκ repertoire and B-cell development, and localizes with condensin on the Igκ locus. *EMBO J.* 32:1168–1182. http://dx.doi.org/10.1038/emboj.2013.66

Pauler, F.M., M.A. Sloane, R. Huang, K. Regha, M.V. Koerner, I. Tamir, A. Sommer, A. Aszodi, T. Jenuwein, and D.P. Barlow. 2009. H3K27me3 forms BLOCs over silent genes and intergenic regions and specifies a histone banding pattern on a mouse autosomal chromosome. *Genome Res.* 19:221–233. http://dx.doi.org/10.1101/gr.080861.108

Peach, S.E., E.L. Rudomin, N.D. Udeshi, S.A. Carr, and J.D. Jaffe. 2012. Quantitative assessment of chromatin immunoprecipitation grade antibodies directed against histone modifications reveals patterns of co-occurring marks on histone protein molecules. *Mol. Cell. Proteomics*. 11:128–137. http://dx.doi.org/10.1074/mcp.M111.015941

Peric-Hupkes, D., W. Meuleman, L. Pagie, S.W. Bruggeman, I. Solovei, W. Brugman, S. Gräf, P. Flicek, R.M. Kerkhoven, M. van Lohuizen, et al. 2010. Molecular maps of the reorganization of genome-nuclear lamina interactions during differentiation. *Mol. Cell*. 38:603–613. http://dx.doi.org/10.1016/j.molcel.2010.03.016

Phillips-Cremins, J.E., M.E.G. Sauria, A. Sanyal, T.I. Gerasimova, B.R. Lajoie, J.S.K. Bell, C.T. Ong, T.A. Hookway, C. Guo, Y. Sun, et al. 2013. Architectural protein subclasses shape 3D organization of genomes during lineage commitment. *Cell*. 153:1281–1295. http://dx.doi.org/10.1016/j.cell.2013.04.053

Reddy, K.L., J.M. Zullo, E. Bertolino, and H. Singh. 2008. Transcriptional repression mediated by repositioning of genes to the nuclear lamina. *Nature*. 452:243–247. http://dx.doi.org/10.1038/nature06727

Renard, E., C. Chadjichristos, M. Kypriotou, G. Beauchef, P. Bordat, A. Dompmartin, R.L. Widom, K. Boumediene, J.P. Pujol, and P. Galéra. 2008. Chondroitin sulphate decreases collagen synthesis in normal and scleroderma fibroblasts through a Smad-independent TGF-β pathway—implication of C-Krox and Sp1. *J. Cell. Mol. Med.* 12(6b):2836–2847. http://dx.doi.org/10.1111/j.1582-4934.2008.00287.x

Reynaud, D., I.A. Demarco, K.L. Reddy, H. Schjerven, E. Bertolino, Z. Chen, S.T. Smale, S. Winandy, and H. Singh. 2008. Regulation of B cell fate commitment and immunoglobulin heavy-chain gene rearrangements by Ikaros. *Nat. Immunol.* 9:927–936. http://dx.doi.org/10.1038/ni.1626

Sandelin, A., W. Alkema, P. Engström, W.W. Wasserman, and B. Lenhard. 2004. JASPAR: an open-access database for eukaryotic transcription factor binding profiles. *Nucleic Acids Res.* 32:D91–D94. http://dx.doi.org/10.1093/nar/gkh012

Sankar, N., S. Baluchamy, R.-K. Kadeppagari, G. Singhal, S. Weitzman, and B. Thimmapaya. 2008. p300 provides a corepressor function by cooperating with YY1 and HDAC3 to repress c-Myc. *Oncogene*. 27:5717–5728. http://dx.doi.org/10.1038/onc.2008.181

Satijn, D.P., K.M. Hamer, J. den Blaauwen, and A.P. Otte. 2001. The polycomb group protein EED interacts with YY1, and both proteins induce neural tissue in *Xenopus* embryos. *Mol. Cell. Biol.* 21:1360–1369. http://dx.doi.org/10.1128/MCB.21.4.1360-1369.2001

Scaffidi, P., and T. Misteli. 2006. Lamin A-dependent nuclear defects in human aging. *Science*. 312:1059–1063. http://dx.doi.org/10.1126/science.1127168

Sehgal, P., P. Chaturvedi, R.I. Kumaran, S. Kumar, and V.K. Parnaik. 2013. Lamin A/C haploinsufficiency modulates the differentiation potential of mouse embryonic stem cells. *PLoS ONE*. 8:e57891. http://dx.doi.org/10.1371/journal.pone.0057891

Seshan, V.E., and A. Olshen. 2014. DNAcopy: DNA copy number data analysis. R package version 1.40.0. http://www.bioconductor.org/packages/release/bioc/manuals/DNAcopy/man/DNAcopy.pdf (accessed December 9, 2014).

Shah, P.P., G. Donahue, G.L. Otte, B.C. Capell, D.M. Nelson, K. Cao, V. Aggarwala, H.A. Cruickshanks, T.S. Rai, T. McBryan, et al. 2013. Lamin B1 depletion in senescent cells triggers large-scale changes in gene expression and the chromatin landscape. *Genes Dev.* 27:1787–1799. http://dx.doi.org/10.1101/gad.223834.113

Shestakova, E.A., Z. Mansuroglu, H. Mokrani, N. Ghinea, and E. Bonnefoy. 2004. Transcription factor YY1 associates with pericentromeric γ-satellite DNA in cycling but not in quiescent (G0) cells. *Nucleic Acids Res.* 32: 4390–4399. http://dx.doi.org/10.1093/nar/gkh737

Simon, M.D., S.F. Pinter, R. Fang, K. Sarma, M. Rutenberg-Schoenberg, S.K. Bowman, B.A. Kesner, V.K. Maier, R.E. Kingston, and J.T. Lee. 2013. High-resolution Xist binding maps reveal two-step spreading during X-chromosome inactivation. *Nature*. 504:465–469. http://dx.doi.org/10.1038/nature12719

Solovei, I., A.S. Wang, K. Thanisch, C.S. Schmidt, S. Krebs, M. Zwerger, T.V. Cohen, D. Devys, R. Foisner, L. Peichl, et al. 2013. LBR and lamin A/C sequentially tether peripheral heterochromatin and inversely regulate differentiation. *Cell*. 152:584–598. http://dx.doi.org/10.1016/j.cell.2013.01.009

Somech, R., S. Shaklai, O. Geller, N. Amariglio, A.J. Simon, G. Rechavi, and E.N. Gal-Yam. 2005. The nuclear-envelope protein and transcriptional repressor LAP2β interacts with HDAC3 at the nuclear periphery, and induces histone H4 deacetylation. *J. Cell Sci.* 118:4017–4025. http://dx.doi.org/10.1242/jcs.02521

Srinivasan, L., and M.L. Atchison. 2004. YY1 DNA binding and PcG recruitment requires CtBP. *Genes Dev.* 18:2596–2601. http://dx.doi.org/10.1101/gad.1228204

Szczerbal, I., H.A. Foster, and J.M. Bridger. 2009. The spatial repositioning of adipogenesis genes is correlated with their expression status in a porcine mesenchymal stem cell adipogenesis model system. *Chromosoma*. 118:647–663. http://dx.doi.org/10.1007/s00412-009-0225-5

Thomas, M.J., and E. Seto. 1999. Unlocking the mechanisms of transcription factor YY1: are chromatin modifying enzymes the key? *Gene*. 236:197–208. http://dx.doi.org/10.1016/S0378-1119(99)00261-9

Towbin, B.D., C. González-Aguilera, R. Sack, D. Gaidatzis, V. Kalck, P. Meister, P. Askjaer, and S.M. Gasser. 2012. Step-wise methylation of histone H3K9 positions heterochromatin at the nuclear periphery. *Cell*. 150: 934–947. http://dx.doi.org/10.1016/j.cell.2012.06.051

Tumbar, T., and A.S. Belmont. 2001. Interphase movements of a DNA chromosome region modulated by VP16 transcriptional activator. *Nat. Cell Biol.* 3:134–139. http://dx.doi.org/10.1038/35055033

Tumbar, T., G. Sudlow, and A.S. Belmont. 1999. Large-scale chromatin unfolding and remodeling induced by VP16 acidic activation domain. *J. Cell Biol.* 145:1341–1354. http://dx.doi.org/10.1083/jcb.145.7.1341

Van Bortle, K., and V.G. Corces. 2012. Nuclear organization and genome function. *Annu. Rev. Cell Dev. Biol.* 28:163–187. http://dx.doi.org/10.1146/annurev-cellbio-101011-155824

Van Bortle, K., and V.G. Corces. 2013. The role of chromatin insulators in nuclear architecture and genome function. *Curr. Opin. Genet. Dev.* 23:212–218. http://dx.doi.org/10.1016/j.gde.2012.11.003

Vella, P., I. Barozzi, A. Cuomo, T. Bonaldi, and D. Pasini. 2012. Yin Yang 1 extends the Myc-related transcription factors network in embryonic stem cells. *Nucleic Acids Res.* 40:3403–3418. http://dx.doi.org/10.1093/nar/gkr1290

Venkatraman, E.S., and A.B. Olshen. 2007. A faster circular binary segmentation algorithm for the analysis of array CGH data. *Bioinformatics*. 23:657–663. http://dx.doi.org/10.1093/bioinformatics/btl646

Verma-Gaur, J., A. Torkamani, L. Schaffer, S.R. Head, N.J. Schork, and A.J. Feeney. 2012. Noncoding transcription within the Igh distal V(H) region at PAIR elements affects the 3D structure of the Igh locus in pro-B cells. *Proc. Natl. Acad. Sci. USA*. 109:17004–17009. http://dx.doi.org/10.1073/pnas.1208398109

Vogel, M.J., D. Peric-Hupkes, and B. van Steensel. 2007. Detection of in vivo protein-DNA interactions using DamID in mammalian cells. *Nat. Protoc.* 2:1467–1478. http://dx.doi.org/10.1038/nprot.2007.148

Wang, J., J. Zhuang, S. Iyer, X. Lin, T.W. Whitfield, M.C. Greven, B.G. Pierce, X. Dong, A. Kundaje, Y. Cheng, et al. 2012. Sequence features and chromatin structure around the genomic regions bound by 119 human transcription factors. *Genome Res.* 22:1798–1812. http://dx.doi.org/10.1101/gr.139105.112

Wei, Z., F. Gao, S. Kim, H. Yang, J. Lyu, W. An, K. Wang, and W. Lu. 2013. Klf4 organizes long-range chromosomal interactions with the oct4 locus in reprogramming and pluripotency. *Cell Stem Cell*. 13:36–47. http://dx.doi.org/10.1016/j.stem.2013.05.010

Wen, B., H. Wu, Y. Shinkai, R.A. Irizarry, and A.P. Feinberg. 2009. Large histone H3 lysine 9 dimethylated chromatin blocks distinguish differentiated from embryonic stem cells. *Nat. Genet.* 41:246–250. http://dx.doi.org/10.1038/ng.297

Wen, B., H. Wu, Y.H. Loh, E. Briem, G.Q. Daley, and A.P. Feinberg. 2012. Euchromatin islands in large heterochromatin domains are enriched for CTCF binding and differentially DNA-methylated regions. *BMC Genomics*. 13:566. http://dx.doi.org/10.1186/1471-2164-13-566

Weth, O., and R. Renkawitz. 2011. CTCF function is modulated by neighboring DNA binding factors. *Biochem. Cell Biol.* 89:459–468. http://dx.doi.org/10.1139/o11-033

Widom, R.L., I. Culic, J.Y. Lee, and J.H. Korn. 1997. Cloning and characterization of hcKrox, a transcriptional regulator of extracellular matrix gene expression. *Gene*. 198:407–420. http://dx.doi.org/10.1016/S0378-1119(97)00360-0

Williams, R.R.E., V. Azuara, P. Perry, S. Sauer, M. Dvorkina, H. Jørgensen, J. Roix, P. McQueen, T. Misteli, M. Merkenschlager, and A.G. Fisher. 2006. Neural induction promotes large-scale chromatin reorganisation of the Mash1 locus. *J. Cell Sci.* 119:132–140. http://dx.doi.org/10.1242/jcs.02727

Wong, X., T.R. Luperchio, and K.L. Reddy. 2014. NET gains and losses: the role of changing nuclear envelope proteomes in genome regulation. *Curr. Opin. Cell Biol.* 28:105–120. http://dx.doi.org/10.1016/j.ceb.2014.04.005

Yang, Q., R. Riblet, and C.L. Schildkraut. 2005. Sites that direct nuclear compartmentalization are near the 5′ end of the mouse immunoglobulin heavy-chain locus. *Mol. Cell. Biol.* 25:6021–6030. http://dx.doi.org/10.1128/MCB.25.14.6021-6030.2005

Yao, J., R.D. Fetter, P. Hu, E. Betzig, and R. Tjian. 2011. Subnuclear segregation of genes and core promoter factors in myogenesis. *Genes Dev.* 25:569–580. http://dx.doi.org/10.1101/gad.2021411

Zlatanova, J., and P. Caiafa. 2009. CTCF and its protein partners: divide and rule? *J. Cell Sci.* 122:1275–1284. http://dx.doi.org/10.1242/jcs.039990

Zuleger, N., S. Boyle, D.A. Kelly, J.I. de las Heras, V. Lazou, N. Korfali, D.G. Batrakou, K.N. Randles, G.E. Morris, D.J. Harrison, et al. 2013. Specific nuclear envelope transmembrane proteins can promote the location of chromosomes to and from the nuclear periphery. *Genome Biol.* 14:R14. http://dx.doi.org/10.1186/gb-2013-14-2-r14

Zullo, J.M., I.A. Demarco, R. Piqué-Regi, D.J. Gaffney, C.B. Epstein, C.J. Spooner, T.R. Luperchio, B.E. Bernstein, J.K. Pritchard, K.L. Reddy, and H. Singh. 2012. DNA sequence-dependent compartmentalization and silencing of chromatin at the nuclear lamina. *Cell*. 149:1474–1487. http://dx.doi.org/10.1016/j.cell.2012.04.035